ELSEVIER

Chemical Engineering Journal 137 (2008) 614–635

Chemical Engineering Journal

www.elsevier.com/locate/cej

An extended macroscopic model for solute dispersion in confined porous media

E. Hamdan, J.F. Milthorpe, J.C.S. Lai *

School of Aerospace, Civil and Mechanical Engineering, University College, University of New South Wales, Australian Defence Force Academy, Canberra 2600, Australia

Received 17 December 2006; received in revised form 26 April 2007; accepted 16 May 2007

Abstract

In the analysis of longitudinal dispersion data in a classical laboratory experiment, it is usually assumed that the dispersion of species undergoes Fickian behaviour with constant dispersivities. If the length and time scales of an experiment are not sufficient for a tracer to traverse the cylinder radius and sample the velocity variations, this could give rise to persisting non-Fickian transients that cannot be predicted by the conventional plug flow dispersion models. Such transients cause the deviation from the Gaussian concentration distribution predicted by the plug models. In this paper, some shortcomings of the Fickian model are examined and a more general non-Fickian macroscopic dispersion model is provided to give insight into some of the factors that contribute to the dispersion process. The analysis describes the transient development of the solute spread and some non-Fickian effects associated with it. The extended model provides a set of conditions under which the classical axial plug dispersion model can be applicable. The model results for tracer dispersion in cylindrical packed beds show that the longitudinal dispersion coefficient converges to its asymptotic value on a time-scale proportional to $R^2/\langle D_T\rangle$ where R is the cylinder radius and $\langle D_T\rangle$ represents the mean value of the radial dispersion coefficient $D_T(r)$ over the cross-section of the bed.

Keywords: Dispersion; Transients; Non-Fickian; Packed bed

1. Introduction

In a typical tracer injection experiment in confined packed beds, the dispersion coefficients are evaluated by fitting the experimental concentration profiles with the plug flow dispersion model solutions. Fickian behaviour of the concentration profile (i.e., a constant dispersion coefficient during solute travel time) is usually assumed. The final results of the fitting are usually expressed in terms of Pe_L versus Pe_m and/or Re_p for various values of Sc. Here Pe_L and Pe_m are Peclet numbers based on the longitudinal dispersion coefficient and molecular diffusion coefficient, respectively, Re_p is the Reynolds number based on the particle diameter and Sc is the Schmidt number. A good review of the work done on evaluating the longitudinal dispersion coefficient, D_L, using the plug dispersion model is provided in Refs. [1,2]. The plug dispersion model has been also used to investigate the dependence of D_L on column and porous media properties such as column dimensions, particle size, particle shape, etc. [1,3,4]. In most cases, except very few, no check has been made on the possible dependence of the dispersion coefficient on the axial position or the possible existence of persisting non-Fickian transients. There are, therefore, doubts about the validity of using the plug dispersion model to interpret experimental dispersion data. The results for solute dispersion in a tube show that a Gaussian distribution of the injected solute is only obtained after a sufficiently long time has elapsed since the release of the solute [5,6]. However and for a variety of reasons (e.g., profiles not measured at a sufficiently long time after the solute injection), the observed concentration profiles are not normally Gaussian. The so-called scale problems do exist and may severely limit the predictive capabilities of the plug dispersion model in evaluating the longitudinal dispersion coefficient.

* Corresponding author. Tel.: +61 2 62688272; fax: +61 2 62688276.
E-mail address: j.lai@adfa.edu.au (J.C.S. Lai).

1385-8947/$ – see front matter © 2007 Elsevier B.V. All rights reserved.
doi:10.1016/j.cej.2007.05.031

Nomenclature

c	concentration of the solute in the gas phase (kg/m^3)
c_0	strength of input pulse (kg/m^3)
C	dimensionless concentration defined in Eq. (3)
d_e	effective diameter defined in Eq. (28)
d_p	particle diameter (m)
d_t	tube diameter (m)
$D_A(r)$	longitudinal dispersion coefficient at radial position r (m^2/s)
$\langle D_A \rangle$	area average longitudinal dispersion coefficient (m^2/s)
D_A^*	dimensionless axial dispersion coefficient defined in Eq. (3)
$\hat{D}_L$	asymptotic longitudinal dispersion in an unconfined packing (m^2/s)
$D_L(\theta)$, $D_L(t)$	time dependent, macroscopic axial dispersion coefficient, plug flow dispersion model in Eq. (16) (m^2/s)
D_L, $D_L(\infty)$	asymptotic value of the longitudinal dispersion coefficient (m^2/s)
D_m	molecular diffusion coefficient (m^2/s)
$D_T(r)$	lateral dispersion coefficient at radial position r (m^2/s)
$\langle D_T \rangle$	area average lateral dispersion coefficient (m^2/s)
D_T^*	dimensionless lateral dispersion coefficient defined in Eq. (3)
$\hat{D}_T$	transverse dispersion rate in an unconfined packing with the same spheres and porosity (m^2/s)
g	a term defined in Eq. (15)
$\bar{g}$	a term defined in Eq. (A.4)
J_0	Bessel function of the zero kind
J_1	Bessel function of the first kind
K_p	porous media permeability (m^2)
l_β	characteristic length defined in Eq. (38)
L	the distance from the point of injection (m)
L^*	pulse dimensionless characteristic length defined
$N(\beta_m)$	$[= 2/J_0^2(\beta_m)]$
Pe_L	Peclet number $\bar{u}d_p/D_L$
Pe_m	Peclet number $\bar{u}d_p/D_m$
Pe_p	Peclet number defined in Eq. (35)
$\widehat{Pe}_p$	Peclet number defined in Eq. (37)
Pe_{Lm}	dimensionless parameter defined in Eq. (3)
Pe_{Rm}	dimensionless parameter defined in Eq. (3)
r	radial co-ordinate (m)
R	tube radius (m)
Re_p	Reynolds number ($= \rho\bar{u}d_p/\mu$).
R_p	particle radius (m)
Re	Reynolds number based on d_e.
Sc	Schmidt number ($=\mu/\rho D_m$).
t	time (s)
t'	dummy variable of integration
$\bar{T}$	integral transform defined in Eq. (A.5)
u	superficial axial velocity (m/s)
u_0	interstitial axial velocity (m/s)
$\bar{u}$	mean axial velocity
$\tilde{u}$	dimensionless axial velocity fluctuation
w	dummy variable of integration
x	dimensionless axial co-ordinate defined in Eq. (3)
x_1	dimensionless axial co-ordinate moving with the mean flow velocity $\bar{u}$
z	axial coordinate (m)

Greek symbols

β_m	eigenvalues of $J_1(\beta_m) = 0$
ε	porous medium porosity

λ	dimensionless variable defined in Eq. (A.4)
μ	dynamic viscosity of the fluid (N s/m^2)
ν	kinematic viscosity of fluid (m^2/s)
θ	dimensionless time defined in Eq. (3)
θ^*	dimensionless time defined in Eq. (34)
$\hat{\theta}$	dimensionless time defined in Eq. (36)
σ	variance of the concentration distribution
τ	a parameter defined in Appendix E.
ζ	dimensionless radial co-ordinate in Eq. (3)

It is worth mentioning that in the groundwater literature, it has been aware for a long time that non-Gaussian behaviour or scale-dependent dispersion coefficients are the norm [7–10]. Non-Fickian behaviour with scale related dispersion coefficients has been studied using various approaches such as stochastic, deterministic and fractal approaches [10,11–14]. Others used Nuclear Magnetic Resonance (NMR) and the random walk method to explain the non-Fickian behaviour for homogeneous and heterogeneous structures [9,15,16]. The scale-dependent dispersion in groundwater hydrology is mainly due to the large scale variations in hydraulic conductivity and the maximum dispersivity is only reached after all variations in the hydraulic conductivity are sampled by the tracer [17].

We will not consider groundwater dispersion in this paper and only consider transient development of solute dispersion in cylindrical beds packed with uniform solid particles (e.g., spherical particles) as is usually the case in packed bed reactors. The porosity in this case shows an oscillatory variation in the radial direction due to the existence of the wall confinement, the so-called "wall effect", and the flow profile exhibits a similar oscillatory behaviour [18,19]. Packed beds are confined and the flow in most applications is non-Darcy which is not usually encountered in groundwater flow.

Non-Fickian behaviour or scale dependent dispersion coefficients are frequently encountered at both laboratory and field scales dispersion experiments, with homogeneous and heterogeneous porous media [8,16,20,21,22]. The possible dependence of the longitudinal dispersion coefficient on the axial position in the packed bed was studied using the axial plug flow dispersion model [4]. According to reference [4], the longitudinal dispersion coefficient is expected to be constant for the dimensionless time θ such that $\hat{\theta} = (L/d_p)(1/\widehat{Pe}_p)(1-\varepsilon)/\varepsilon \gg 0.3$. Recent developments in the experimental techniques such as NMR spectrometer and particle imaging have allowed researchers to measure the temporal and spatial tracer development at the pore level [23–27]. In parallel, advances in the computational power allow pore–scale flow and tracer dispersion to be simulated by implementing numerical techniques such as Lattice–Boltzman (LB) and random walk particle tracking methods [19,28,29]. However, there are limitations associated with such experimental and computational techniques. NMR experiments, for example, are limited by the signal decay and are usually performed using cylindrical packed beds with lengths in the range between $50d_p$–$100d_p$. Computational limitations and the level of accuracy required restrict pore–scale simulation to beds of smaller sizes than those usually used in NMR experiments (i.e., cylinders with radius $R < 10d_p$ [19], where d_p is the particle diameter). Therefore, pore–scale simulation is considered to be a reliable tool only for short time analysis of the dispersion process (i.e., $t < 20d_p/\bar{u}$) where $\bar{u}$ is the mean longitudinal velocity in the bed. This time scale is very short when compared to the time required for a typical tracer injection experiment or the mass transport process in most packed bed reactors [30]. Therefore, there is still the need to introduce developments to the existing dispersion models at both the pore–scale and macroscopic scale to improve their ability in evaluating the asymptotic dispersion rates and to be able to capture any possible non-Fickian transients.

In this paper, we will extend the conventional axial plug flow dispersion model by including additional transient higher order dispersion terms, usually neglected under the Fickian assumption, that contribute to the deviation from Guassianity. In doing so, we aim to provide a more comprehensive picture of the dispersion process by providing a better description of the different dispersion mechanisms taking place and show how they affect the time scales needed to reach Gaussinity. The extensions will introduce a set of criteria equations other than those proposed in refs. [4,31] for using the plug dispersion models. A new criterion equation on the bed length will be derived and validated against the conditions used in previous experiments which adopt the conventional plug dispersion models in their analysis and also against recent pore–scale simulation results which take into account the so called "wall effect" [19,33]. In this manner, the extended macroscopic non-Fickian model will establish a cross-link between the detailed pore–scale simulation results and the macroscopic treatment of the dispersion process and passing information between the two levels. Transient effects associated with the non-mechanical dispersion mechanisms (e.g., hold up and boundary layer dispersion mechanisms [32]) will not be considered in this study. In sphere packings, mechanical sources dominate longitudinal dispersion and there is no experimental evidence that shows a significant contribution of the hold-up dispersion in the case of impermeable particles [33]. We will apply the model to study solute dispersion in a confined bed of randomly packed spherical particles. The heterogeneities in the packing will only be a result of the wall confinement and for simplicity, we will assume the Darcy model to be valid.

2. Problem formulation

The basic mass transport equation for solute dispersion in cylindrical packed beds under conditions of radial flow non-uniformity is given by [34]

$$\frac{\partial c}{\partial t} + u_0(r)\frac{\partial c}{\partial z} = D_A(r)\frac{\partial^2 c}{\partial z^2} + \frac{1}{r}\frac{\partial}{\partial r}\left(rD_T(r)\frac{\partial c}{\partial r}\right) \tag{1}$$

or, referring to the empty cross-section

$$\varepsilon\frac{\partial c}{\partial t} + u(r)\frac{\partial c}{\partial z} = \varepsilon D_A(r)\frac{\partial^2 c}{\partial z^2} + \frac{1}{r}\frac{\partial}{\partial r}\left(r\varepsilon D_T(r)\frac{\partial c}{\partial r}\right) \tag{2}$$

where u is the superficial velocity ($u = \varepsilon u_0$) and ε is the porosity. Since the axial and radial dispersion coefficients D_A and D_T are functions of the fluctuating flow profile and molecular diffusion effect, they are also functions of the radial position [31,34]. We make Eq. (2) dimensionless by defining the following non-dimensional variables

$$C = \frac{c}{c_0}, \quad x = \frac{z}{R}, \quad \theta = \frac{\bar{u}t}{R}, \quad D_T^* = \frac{D_T}{\langle D_T\rangle}, \quad D_A^* = \frac{D_A}{\langle D_A\rangle}, \quad \zeta = \frac{r}{R}, \quad Pe_{Lm} = \frac{\bar{u}R}{\langle D_A\rangle}, \quad Pe_{Rm} = \frac{\bar{u}R}{\langle D_T\rangle} \tag{3}$$

where $\langle D_T\rangle$ and $\langle D_A\rangle$ are the area averaged values of D_T and D_A over the bed cross-section defined as $[\langle D_T\rangle = (2/R^2)\int_0^R rD_T(r)\,dr]$ and $[\langle D_A\rangle = (2/R^2)\int_0^R rD_A(r)\,dr]$, respectively. D_A^* and D_T^* are the dispersion coefficients $D_A(r)$ in the longitudinal direction and $D_T(r)$ in the transverse direction normalised by their area-averaged values. The dimensionless time θ measures the time for the transport of the tracer downstream by the mean flow velocity u. Pe_{Lm}, the Peclet number for the bed, represents the ratio between advective and dispersive mechanisms quantified by the average longitudinal dispersion coefficient $\langle D_A\rangle$. Pe_{Rm} on the other hand is the Peclet number which represents the ratio between advective and dispersive mechanisms quantified by the average transverse dispersion coefficient $\langle D_T\rangle$.

Substituting Eq. (3) into Eq. (2) yields

$$\varepsilon\frac{\partial C}{\partial\theta} = -\frac{u}{\bar{u}}\frac{\partial C}{\partial x} + \varepsilon\frac{D_A^*}{Pe_{Lm}}\frac{\partial^2 c}{\partial x^2} + \frac{1}{Pe_{Rm}}\frac{1}{\zeta}\frac{\partial}{\partial\zeta}\left(\zeta\varepsilon D_T^*\frac{\partial C}{\partial\zeta}\right) \tag{4}$$

The concentration C, flow velocity u, local dispersion coefficients (D_A^* and D_T^*) and porosity ε can be expressed in terms of their area averaged values ($\bar{C}$, $\bar{u}$, $\bar{D}_A^*$, $\bar{D}_T^*$, $\bar{\varepsilon}$) and fluctuations ($\tilde{C}$, $\tilde{u}$, $\tilde{D}_A^*$, $\tilde{D}_T^*$, $\tilde{\varepsilon}$) from the area averages as

$$C = \bar{C} + \tilde{C} \tag{5}$$

$$u = \bar{u} + \tilde{u} \tag{6}$$

$$D_A^* = \bar{D}_A^* + \tilde{D}_A^* \tag{7}$$

$$D_T^* = \bar{D}_T^* + \tilde{D}_T^* \tag{8}$$

$$\varepsilon = \bar{\varepsilon} + \tilde{\varepsilon} \tag{9}$$

where

$$\overline{\tilde{C}} = \overline{\tilde{u}} = \overline{\tilde{D}}_A^* = \overline{\tilde{D}}_T^* = \overline{\tilde{\varepsilon}} = 0 \tag{10}$$

Substituting Eqs. (5)–(9) into Eq. (4), taking the area average of the resulting equation and making use of Eq. (10) and the boundary condition $\partial\tilde{c}/\partial\xi|_{\xi=1} = 0$, the transport equation for $\bar{C}$ when expressed in terms of the moving coordinate $x_1 = x - \bar{u}\theta$ is

$$\bar{\varepsilon}\frac{\partial\bar{C}}{\partial\theta} = -\frac{\partial}{\partial x_1}(\overline{\tilde{u}\tilde{C}}) - \frac{\partial(\overline{\tilde{\varepsilon}\tilde{C}})}{\partial\theta} + \frac{1}{Pe_{Lm}}\left[\bar{\varepsilon}\frac{\partial^2\bar{C}}{\partial x_1^2} + \bar{\varepsilon}\frac{\partial^2\overline{(\tilde{D}_A^*\tilde{C})}}{\partial x_1^2} + \frac{\partial^2\overline{(\tilde{\varepsilon}\tilde{C})}}{\partial x_1^2} + (\overline{\tilde{\varepsilon}\tilde{D}_A^*})\frac{\partial^2\bar{C}}{\partial x_1^2} + \frac{\partial^2\overline{(\tilde{\varepsilon}\tilde{D}_A^*\tilde{C})}}{\partial x_1^2}\right] \tag{11}$$

The quantity $(\overline{\tilde{u}\tilde{C}})$ is the axial component of the dispersion that represents the flux associated with the correlation between the fluctuations in velocity, $\tilde{u}$, and concentration, $\tilde{C}$, relative to their averaged values. The new quantity $\overline{(\tilde{D}_A^*\tilde{C})}$ is the additional contribution to dispersion caused by deviations in the local dispersion coefficients.

The equation describing the concentration perturbation $\tilde{C}$ is obtained by substracting Eq. (11) from Eq. (4) as

$$\begin{aligned}\bar{\varepsilon}\frac{\partial\tilde{C}}{\partial\theta}+\tilde{\varepsilon}\frac{\partial\bar{C}}{\partial\theta}&=-\tilde{u}\frac{\partial\bar{C}}{\partial x_1}+\frac{\bar{\varepsilon}}{Pe_{\mathrm{Lm}}}\frac{\partial^2\tilde{C}}{\partial {x_1}^2}+\frac{\bar{\varepsilon}}{Pe_{\mathrm{Rm}}}\left[\frac{1}{\zeta}\frac{\partial}{\partial\zeta}\left(\zeta\frac{\partial\tilde{C}}{\partial\zeta}\right)+\frac{1}{\zeta}\frac{\partial}{\partial\zeta}\left(\zeta\tilde{D}_{\mathrm{T}}^{*}\frac{\partial\tilde{C}}{\partial\zeta}\right)\right]\\&+\frac{1}{Pe_{\mathrm{Rm}}}\left[\frac{1}{\zeta}\frac{\partial}{\partial\zeta}\left(\zeta\tilde{\varepsilon}\frac{\partial\tilde{C}}{\partial\zeta}\right)+\frac{1}{\zeta}\frac{\partial}{\partial\zeta}\left(\zeta\tilde{\varepsilon}\tilde{D}_{\mathrm{T}}^{*}\frac{\partial\tilde{C}}{\partial\zeta}\right)\right]+\left[\frac{\tilde{\varepsilon}}{Pe_{\mathrm{Lm}}}+\frac{\bar{\varepsilon}\,\tilde{D}_{\mathrm{A}}^{*}}{Pe_{\mathrm{Lm}}}\right]\frac{\partial^2\bar{C}}{\partial {x_1}^2}-\frac{\partial}{\partial x_1}\underbrace{[\overline{(\tilde{u}\tilde{C})}-\tilde{u}\tilde{C}]}_{\mathrm{I}}\\&-\frac{\partial}{\partial\theta}\underbrace{[\tilde{\varepsilon}\tilde{C}-\overline{(\tilde{\varepsilon}\tilde{C})}]}_{\mathrm{II}}+\frac{\bar{\varepsilon}}{Pe_{\mathrm{Lm}}}\frac{\partial}{\partial {x_1}^2}\underbrace{[\tilde{D}_{\mathrm{A}}^{*}\tilde{C}-\overline{(\tilde{D}_{\mathrm{A}}^{*}\tilde{C})}]}_{\mathrm{III}}+\frac{1}{Pe_{\mathrm{Lm}}}\frac{\partial}{\partial {x_1}^2}\underbrace{[\tilde{\varepsilon}\tilde{C}-\overline{(\tilde{\varepsilon}\tilde{C})}]}_{\mathrm{IV}}+\frac{1}{Pe_{\mathrm{Lm}}}\frac{\partial}{\partial {x_1}^2}\underbrace{[\tilde{\varepsilon}\tilde{D}_{\mathrm{A}}^{*}\tilde{C}-\overline{(\tilde{\varepsilon}\tilde{D}_{\mathrm{A}}^{*}\tilde{C})}]}_{\mathrm{V}}\\&+\frac{1}{Pe_{\mathrm{Lm}}}\underbrace{[\tilde{\varepsilon}\tilde{D}_{\mathrm{A}}^{*}-\overline{(\tilde{\varepsilon}\tilde{D}_{\mathrm{A}}^{*})}]}_{\mathrm{VI}}\frac{\partial^2\bar{C}}{\partial {x_1}^2}\end{aligned}\tag{12}$$

where $\tilde{u}$ in Eq. (12) is normalized by $\bar{u}$. For small perturbations and neglecting triplet perturbed quantities that could result when multiplying Eq. (12) by $\tilde{u}$ or $\tilde{D}_{\mathrm{A}}^{*}$ to solve for the terms $(\overline{\tilde{u}\tilde{C}})$ and $(\overline{\tilde{D}_{\mathrm{A}}^{*}\tilde{C}})$, the final approximate form of the perturbed concentration equation to be solved may be written as

$$\bar{\varepsilon}\frac{\partial\tilde{C}}{\partial\theta}+\tilde{\varepsilon}\frac{\partial\bar{C}}{\partial\theta}=-\tilde{u}\frac{\partial\bar{C}}{\partial x_1}+\frac{\bar{\varepsilon}}{Pe_{\mathrm{Lm}}}\frac{\partial^2\tilde{C}}{\partial x_1^2}+\frac{\bar{\varepsilon}}{Pe_{\mathrm{Rm}}}\left[\frac{1}{\zeta}\frac{\partial}{\partial\zeta}\left(\zeta\frac{\partial\tilde{C}}{\partial\zeta}\right)\right]+\left[\frac{\tilde{\varepsilon}}{Pe_{\mathrm{Lm}}}+\frac{\bar{\varepsilon}\,\tilde{D}_{\mathrm{A}}^{*}}{Pe_{\mathrm{Lm}}}\right]\frac{\partial^2\bar{C}}{\partial x_1^2}\tag{13}$$

Eq. (13) can be re-written as

$$\frac{\partial\tilde{C}}{\partial\theta}=\frac{1}{Pe_{\mathrm{Lm}}}\frac{\partial^2\tilde{C}}{\partial x_1^2}+\frac{1}{Pe_{\mathrm{Rm}}}\left[\frac{1}{\zeta}\frac{\partial}{\partial\zeta}\left(\zeta\frac{\partial\tilde{C}}{\partial\zeta}\right)\right]+g(x_1,\theta,\zeta)\tag{14}$$

where

$$g(x_1,\theta,\zeta)=-\frac{\tilde{u}}{\bar{\varepsilon}}\frac{\partial\bar{C}}{\partial x_1}+\left[\frac{\tilde{\varepsilon}}{\bar{\varepsilon}Pe_{\mathrm{Lm}}}+\frac{\tilde{D}_{\mathrm{A}}^{*}}{Pe_{\mathrm{Lm}}}\right]\frac{\partial^2\bar{C}}{\partial x_1^2}\tag{15}$$

Eq. (14) is solved using the integral transform technique [35] as shown in Appendix A. The final mean solute concentration equation can be written as

$$\frac{\partial\bar{C}}{\partial\theta}=K_0(\theta)\frac{\partial^2\bar{C}}{\partial x_1^2}+K_1(\theta)\frac{\partial^2\bar{C}}{\partial x_1\partial\theta}+K_2(\theta)\frac{\partial^3\bar{C}}{\partial x_1^3}+K_3(\theta)\frac{\partial^3\bar{C}}{\partial x_1^2\partial\theta}+K_4(\theta)\frac{\partial^4\bar{C}}{\partial x_1^4}+K_5(\theta)\frac{\partial^4\bar{C}}{\partial x_1^3\partial\theta}+\cdots\tag{16}$$

where $K_0(\theta)$–$K_5(\theta)$ are time variable coefficients defined in Appendix B. The most important coefficients are $K_0(\theta)$ (the effective axial dispersion coefficient in the bed), $K_2(\theta)$ (representing the contribution of $\tilde{u}$, $\tilde{D}_{\mathrm{A}}^{*}$ and $\tilde{\varepsilon}$ in the bed to the distribution skewness) and $K_3(\theta)$ and $K_4(\theta)$ (representing the contribution of $\tilde{u}$, $\tilde{D}_{\mathrm{A}}^{*}$ and $\tilde{\varepsilon}$ to the distribution flatness). As will be shown later, as time becomes larger and larger, the transient coefficients $K_0(\theta)$–$K_5(\theta)$ in Eq. (16) reach their asymptotic behaviour and Eq. (16) reduces to

$$\frac{\partial\bar{C}}{\partial\theta}=K_0(\infty)\frac{\partial^2\bar{C}}{\partial x_1^2}+K_1(\infty)\frac{\partial^2\bar{C}}{\partial x_1\partial\theta}+K_2(\infty)\frac{\partial^3\bar{C}}{\partial x_1^3}+K_3(\infty)\frac{\partial^3\bar{C}}{\partial x_1^2\partial\theta}+K_4(\infty)\frac{\partial^4\bar{C}}{\partial x_1^4}+K_5(\infty)\frac{\partial^4\bar{C}}{\partial x_1^3\partial\theta}+\cdots\tag{17}$$

The asymptotic coefficients $K_0(\infty)$–$K_5(\infty)$ are defined in Appendix B.

It is clear from Eq. (17) that attaining the asymptotic behaviour of $K_0(\theta)$–$K_5(\theta)$ does not mean that the effect of higher order derivatives of $\bar{C}$ on the distribution profile (e.g., skewness and flatness) is minimized/neglected. Therefore and as will be discussed later, additional conditions have to be satisfied to minimize/neglect their effects.

Without the dispersion term $\partial^3\bar{C}/\partial x_1^2\partial\theta$, the transport equation for large time analysis, Eq. (17), is similar to that obtained in ref. [34]. Therefore, the Carbonell dispersion model [34] cannot provide information on the temporal development of the dispersion coefficients and does not shed light on the factors contributing to the deviation from the normal distribution. It is worth mentioning that the general form of the transport Eq. (16) is similar to that obtained using the stochastic analysis to describe solute dispersion in stratified (hydraulic conductivity varies only in one direction) aquifer [10].

3. Analysis and results

To simplify our analysis, we will restrict ourselves to the application of Eq. (1) referring to the cross-section of the fluid phase (we set $\tilde{\varepsilon}=0$ and $\bar{\varepsilon}=1$ in $K_0(\theta)$–$K_5(\theta)$ equations in Appendix B). The temporal development of the effective axial dispersion coefficient

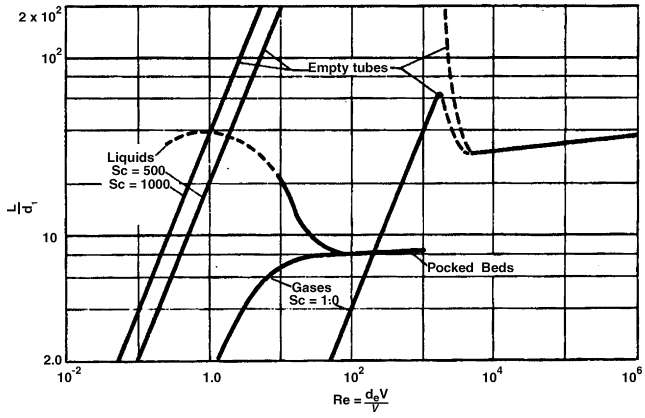

Fig. 1. Restriction on length to diameter ratio of equipment if the dispersed plug flow models are to be applicable (at $d_t/d_p = 15$ and $\varepsilon = 0.38$), "Reprinted from ref. [31], p. 263, Copyright (2005), with permission from Elsevier".

$D_L(\theta)$ when expressed as a ratio of its asymptotic value $D_L(\infty)$ is given by

$$\frac{D_L(\theta)}{D_L(\infty)} = \frac{\sum_{m=1}^{\infty} \overline{\tilde{u} J_0(\beta_m, \zeta)}/(N(\beta_m))((1 - e^{-\lambda\theta})/\lambda) \int_0^1 \zeta J_0(\beta_m, \zeta)\tilde{u}\, d\zeta + (1/Pe_{Lm})}{\sum_{m=1}^{\infty} \overline{\tilde{u} J_0(\beta_m, \zeta)}/(\lambda N(\beta_m)) \int_0^1 \zeta J_0(\beta_m, \zeta)\tilde{u}\, d\zeta + (1/Pe_{Lm})} \tag{18}$$

The temporal development of the fourth term to the right hand side of Eq. (16) defined by $V(\theta)$, which contributes to the flatness of the concentration profile can be normalised by its asymptotic value $V(\infty)$ (see Appendix B) as

$$\frac{V(\theta)}{V(\infty)} = \frac{\sum_{m=1}^{\infty} \overline{\tilde{u} J_0(\beta_m, \zeta)}/(N(\beta_m))((1 - (1 + \lambda\theta)e^{-\lambda\theta})/\lambda^2) \int_0^1 \zeta J_0(\beta_m, \zeta)\tilde{u}\, d\zeta}{\sum_{m=1}^{\infty} \overline{\tilde{u} J_0(\beta_m, \zeta)}/(\lambda^2 N(\beta_m)) \int_0^1 \zeta J_0(\beta_m, \zeta)\tilde{u}\, d\zeta} \tag{19}$$

The asymptotic axial dispersion coefficient $D_L(\infty)$ in Eq. (18) reduces to essentially the same one for solute dispersion in empty tubes [i.e., $1/Pe = 1/Pe_{Lm} + hPe_{Rm}$; h (the velocity constant) = 1/48 and $Pe = \bar{u}R/D_L(\infty)$] [5,6]. When using the approximation proposed in ref. [36] for the velocity profile in a cylindrical packed bed,we obtain the value of $h = 1/1230$ which is approximately equal to the value of $h = 0.0008$ obtained in ref. [31]. Looking at different transient terms (see Appendix B) in Eq. (16), it is possible to obtain the necessary restrictions for such transients to become time-independent:

$$O(e^{-\lambda\theta}) \ll 1 \tag{20}$$

and

$$O((1 + \lambda\theta)e^{-\lambda\theta}) \ll 1 \tag{21}$$

The condition in Eq. (20) is the same as that proposed in ref. [31]. The condition in Eq. (21) results from the transient dispersion terms which contain the function $1-(1+\lambda\theta)e^{-\lambda\theta}$. One can express such restrictions in terms of equipment dimensions. If a ratio of 10:1 is taken for the inequalities in Eqs. (20) and (21) [31], the approximate conditions to be fulfilled are:

$$e^{-\lambda\theta} \approx 0.1 \tag{22}$$

and

$$(1 + \lambda\theta)e^{-\lambda\theta} \approx 0.1 \tag{23}$$

The condition in Eq. (22) yields

$$\frac{L}{d_t} > 0.04(Re)\frac{d_t}{d_e}\frac{\nu}{\langle D_T\rangle} \tag{24}$$

Fig. 1 shows the restrictions on equipment L/d_t ratio according to criterion Eq. (24) for the cases of an empty tube and a packed bed with $d_t/d_p = 15$ and $\varepsilon = 0.38$ [31]. The condition in Eq. (23) requires the solution of the equation

$$14.7\theta^* = \ln(10 + 147\theta^*) \tag{25}$$

where

$$\theta^* = \frac{L\langle D_T\rangle}{(\bar{u}R^2)} = \frac{\langle D_T\rangle t}{(R^2)} \tag{26}$$

and θ^* represents the dimensionless dispersion time. $L/\bar{u}$ represents the characteristic time for a dispersion experiment and $\langle D_T\rangle/R^2$ scale measures the time for the transverse transport quantified by $\langle D_T\rangle$. The solution of Eq. (25) is $\theta^* = 0.264$ which yields

$$\frac{L}{d_t} > 0.06(Re)\frac{d_t}{d_e}\frac{\nu}{\langle D_T\rangle} \tag{27}$$

where d_e represents the effective or hydraulic diameter (4 × free volume of fluid/wetted area) [31]. It is used as a characteristic length in the dimensionless number d_e/d_t defined as [31]

$$\frac{d_e}{d_t} = \frac{\varepsilon d_t}{3/2(d_t/d_p)(1-\varepsilon)+1} \tag{28}$$

Re is the Reynolds number based on d_e. For comparison, Taylor criterion for dispersion in a tube could be written as

$$\frac{L}{d_t} > 0.06(Re)\frac{\nu}{D_m} \tag{29}$$

where for empty tubes $\varepsilon = 1$, hence $d_t = d_e$. Therefore, the criterion given by Eq. (27) reduces to that obtained for dispersion in empty tubes where $\langle D_T\rangle = D_m$ [5]. Note that the final value of θ^* and in turn the constant value in Eq. (27) depends on the required accuracy level (i.e., the ratio taken for the inequalities in Eqs. (20) and (21)). From the previous analysis, we make the following conclusions.

- The time-scale for attaining the asymptotic longitudinal dispersion rates in a packed cylinder is neither the convective ($t \propto d_p/\bar{u}$) nor the diffusive ($t \propto d_p/D_m$) time-scales but is proportional to $R^2/\langle D_T\rangle$. This result is in accordance with the pore–scale simulations for tracer dispersion in a fluid flowing through a cylindrical monodisperse sphere packing [19,30].
- Comparing Eq. (24) with Eq. (27) shows a difference in the L/d_t ratio by a factor of 1.5. Therefore, the data in Fig. 1 should be corrected by a correction factor of 1.5 in order for all the dispersion coefficients in Eq. (16) to become time-independent.
- If criterion Eq. (27) is satisfied, our extended dispersion model for large time analysis reduces to that given by Eq. (17). However, the reduced dispersion model still contains extra dispersion terms when compared with the classical axial plug dispersion model. Such terms are expected to contribute to the deviation from the normal Gaussian distribution even at longer times after the introduction of the solute. For example, the third term to the right hand side of Eq. (17) will contribute to the skewness of the pulse while the second and fourth terms to the right hand side of Eq. (17) will contribute to the distribution flatness. The classical axial plug dispersion model only includes the first two terms of Eq. (17) (i.e., $\partial\bar{C}/\partial\theta$ and $\partial^2\bar{C}/\partial x_1^2$) and therefore, additional conditions must be satisfied to avoid skewness and peakedness of the pulse.

Looking at the order of magnitude estimates of the terms (see Appendix B) to the right hand side of Eq. (17), we make the following conclusions.

- The second derivative term will dominate the third derivative in x_1 if the condition

$$\frac{Pe_{Lm}\sum_{m=1}^{\infty}\overline{\tilde{u}J_0(\beta_m,\zeta)}/(\lambda N(\beta_m))\int_0^1\zeta J_0(\beta_m,\zeta)\tilde{u}\,d\zeta + 1}{\sum_{m=1}^{\infty}\overline{\tilde{D}_L^* J_0(\beta_m,\zeta)}/(\lambda N(\beta_m))\int_0^1\zeta J_0(\beta_m,\zeta)\tilde{u}\,d\zeta + \sum_{m=1}^{\infty}\overline{\tilde{u}J_0(\beta_m,\zeta)}/(\lambda N(\beta_m)) + \int_0^1\zeta J_0(\beta_m,\zeta)\tilde{D}_L^*\,d\zeta}L^* \gg 1 \tag{30}$$

  is satisfied where L^* is some reference dimensionless pulse length [34] which increases with time, and may be chosen to be the pulse length relative to the initial pulse width.
- The second derivative term will dominate the fourth derivative in x_1 if the condition,

$$\frac{Pe_{Lm}\sum_{m=1}^{\infty}\overline{\tilde{u}J_0(\beta_m,\zeta)}/(\lambda N(\beta_m))\int_0^1\zeta J_0(\beta_m,\zeta)\tilde{u}\,d\zeta + 1}{\sum_{m=1}^{\infty}\overline{\tilde{u}J_0(\beta_m,\zeta)}/\lambda^2 N(\beta_m)\int_0^1\zeta J_0(\beta_m,\zeta)\tilde{u}d\zeta + \sum_{m=1}^{\infty}\overline{\tilde{D}_L^* J_0(\beta_m,\zeta)}/(\lambda N(\beta_m))\int_0^1\zeta J_0(\beta_m,\zeta)\tilde{D}_L^*d\zeta}L^{*2} \gg 1 \tag{31}$$

  is satisfied.
- The second derivative term will dominate the third derivative term in x_1 and θ for times such that

$$\frac{\sum_{m=1}^{\infty}\overline{\tilde{u}J_0(\beta_m,\zeta)}/(\lambda N(\beta_m))\int_0^1\zeta J_0(\beta_m,\zeta)\tilde{u}\,d\zeta + 1/(Pe_{Lm})}{\sum_{m=1}^{\infty}\overline{\tilde{u}J_0(\beta_m,\zeta)}/(\lambda^2 N(\beta_m))\int_0^1\zeta J_0(\beta_m,\zeta)\tilde{u}\,d\zeta}\theta \gg 1 \tag{32}$$

  is satisfied.
- The second derivative term will dominate the fourth derivative term in x_1 and θ for times such that

$$\frac{Pe_{Lm}\sum_{m=1}^{\infty}\overline{\tilde{u}J_0(\beta_m,\zeta)}/(\lambda N(\beta_m))\int_0^1\zeta J_0(\beta_m,\zeta)\tilde{u}\,d\zeta + 1}{\sum_{m=1}^{\infty}\overline{\tilde{D}_L^* J_0(\beta_m,\zeta)}/(\lambda^2 N(\beta_m))\int_0^1\zeta J_0(\beta_m,\zeta)\tilde{u}\,d\zeta}L^*\theta \gg 1 \tag{33}$$

The Peclet number Pe_{Lm} is normally greater than 1 and the pulse characteristic length L^* increases with time and is at least of order 1. Criteria Eqs. (30)–(33) can now be approximately represented in terms of the order of magnitudes of the Peclet flow parameters only as shown in Appendix C. Note that criterion (C.1) (or (30)) should be satisfied in order for the term contributing to the pulse skewness to be neglected relative to dispersion in the axial direction while criteria (C.2) and (C.3) (or (31) and (32)) should be satisfied in order for the terms contributing to the pulse flatness to be neglected relative to dispersion in the axial direction. Criteria Eqs. (C.1)–(C.4) in Appendix C show that

- At large values of Pe_{Rm} and Pe_{Lm} and as time becomes larger and larger, criteria Eqs. (C.1) and (C.2) are easier to meet than criteria Eqs. (C.3) and (C.4).
- Comparing criteria Eqs. (C.1) and (C.2) and due to the dependence on L^{*2}, it is expected that criterion Eq. (C.2) is easier to satisfy as the time increases especially at low Pe_{Rm} values.
- Criterion Eq. (C.1) must be satisfied if the skewness effect is to be neglected while criteria Eqs. (C.2) and (C.3) should be met to avoid pulse flatness.
- Comparing criteria Eqs. (C.3) and (C.4) it is clear that at larger times, criterion Eq. (C.4) is much easier to satisfy than criterion Eq. (C.3). Therefore, it is expected that the persisting flatness of the pulse will be merely due to the difficulty in satisfying criterion Eq. (C.3).

Since there were some approximations involved in the derivation of criteria Eqs. (21)–(29) and Eqs. (C.1)–(C.4), they should be considered to be order of magnitude estimations.

To compare criterion Eq. (27) with Han's criterion [4], criterion Eq. (27) can be re-written as

$$\theta^* = \left(\frac{L}{d_P}\right)\frac{1}{Pe_p}\left(\frac{d_p}{R}\right)^2 \geq 0.2646 \tag{34}$$

where

$$Pe_p = \frac{\bar{u}d_p}{\langle D_T\rangle} \tag{35}$$

is the particle Peclet number. Criterion Eq. (34) clearly shows that for high Pe_p numbers, one needs larger L/d_p ratios to attain the asymptotic longitudinal dispersion coefficient. For comparison, the time constraint obtained from the experimental observations in ref. [4] showed that one can expect a constant longitudinal dispersivity as long as

$$\hat{\theta} = \left(\frac{L}{d_P}\right)\frac{1}{\widehat{Pe}_p}\left(\frac{1-\varepsilon}{\varepsilon}\right) \geq 0.3 \tag{36}$$

where

$$\widehat{Pe}_p = \frac{\bar{u}l_\beta}{D_m} \tag{37}$$

is the Peclet number based on a characteristic length l_β associated with the pore spaces in the fluid–solid system [4] instead of the tube radius R, where

$$l_\beta = d_p\left(\frac{\varepsilon}{1-\varepsilon}\right) \tag{38}$$

Criterion Eq. (34) reduces to criterion Eq. (36) when using the characteristic length scale l_β and setting $\langle D_T\rangle = D_m$. However, the rigorous scaling Eq. (36) is in apparent conflict with the time scales obtained from the NMR analysis and pore–scale simulation results [23,30]. In the former, criterion Eq. (36) overestimated the asymptotic time scales and in the latter, the time scales in confined beds were found to be proportional to R^2 and $\hat{D}_T$, where $\hat{D}_T$ represents the transverse dispersion rate in an unconfined packing with the same spheres and porosity [19,30]. The present analysis includes $D_A(r)$ and $D_T(r)$ instead of D_m in Eq. (1). Except for very low Reynolds flow, the time scales proportional to $R^2/\langle D_T\rangle$ as the case in packed beds are much smaller than those proportional to R^2/D_m as established in some of the studies [37–41] to be the time scale to converge to the asymptotic Taylor dispersion coefficient. This can be clearly seen from inspection of Fig. 1 that the L/d_t ratio for laminar flow of liquids in empty tubes is much larger than that for packed beds. Furthermore, the asymptotic time scales also depend on the packing geometry and whether the packing is confined or not. For example, simulation results for unconfined random packing of spheres show that the asymptotic dispersion was attained on a convective time scale proportional to $d_p/\bar{u}$ and when introducing the wall confinement to the packing, the asymptotic time scale is proportional to $R^2/\langle D_T\rangle$ [19,23]. On the other hand, the asymptotic time scale in a periodic array of spheres is proportional to d_p^2/D_m [30,33]. It is worth mentioning that in the majority of investigations, including [4], which deals with evaluating the asymptotic D_L, it is usually assumed that the concentration gradient in the axial direction is so steep that the radial concentration gradient can be

neglected. However, our results and the pore–scale simulation findings [19,30], show that the time scale for attaining the asymptotic value of D_L is proportional to $R^2/\langle D_T\rangle$. This means that the asymptotic rates to attain constant D_L grow significantly with R and are at the same time dependent on $\langle D_T\rangle$, usually neglected in a typical tracer injection experiment for the evaluation of D_L. Table 1 shows some experimental conditions to evaluate D_L using the classical plug dispersion model. The data needed for our calculations in Table 1 has been obtained directly from [2]. The equipment dimension constraint L/d_t in Table 1 is evaluated using criterion Eq. (27) which could be re-written as

$$\frac{L}{d_t} > 0.06\,Pe_p\frac{d_t}{d_p} \tag{39}$$

In most experiments which use the plug dispersion model, the longitudinal and lateral dispersion coefficients are evaluated separately. To be able to apply criterion Eq. (39), the values of Pe_p should be evaluated beforehand. The approximate values of Pe_p were calculated using the data and the empirical correlations in the literature [2]. Here, we assume that the plug dispersion model usually used for the evaluation of Pe_p is applicable and $D_T = \langle D_T\rangle =$ constant. It is worth mentioning that criterion Eq. (34) is derived on the basis of attaining time-independent dispersion coefficients in Eq. (16) and the asymptotic time scale to reach a constant traverse dispersion coefficient is usually less than that suggested by Eq. (34). It is quite clear from Tables 1 and 2 that the following observations can be made.

- In the majority of the experiments for evaluating D_L of liquids in packed beds, criterion Eq. (39) is either marginally satisfied (especially at low Reynolds flows) or not satisfied at all. This is especially true for the experiments in references [4,45,46,48,49,51,53,54]. This indicates that the axial dispersion coefficients under the reported experimental conditions are still in the transient development regime. Hence in these cases, the plug dispersion model is not applicable for the analysis of the experimental results.
- The experiments in references [42,47,52,56–58] satisfy the length criterion in Eq. (39) for the entire range of Reynold numbers used. The results in Tables 1 and 2 also show that high Reynolds number flows require larger L/d_p ratios in order for criterion Eq. (39) to be satisfied.
- The results in Table 2 show that criterion Eq. (39) is easier to satisfy for the case of gases in packed beds in accordance with the early findings for solute dispersion in tubes [5].

Except in Ref. [4], no systematic effort was made by researchers to study the possible dependence of the longitudinal dispersion coefficient on the axial position. Furthermore, the experimental conditions under which criterion Eq. (36) was obtained do not satisfy the proposed criterion Eq. (39). This raises justifiable doubts regarding the validity of criterion Eq. (36) which was also criticised by others [19,23]. In fact, in the derivation of criterion Eq. (36), the standard plug dispersion model was used to analyse the dispersion data and to investigate the dependence of D_L on position [4], which is inappropriate. Despite that, many researchers adopted criterion Eq. (36) or used large d_t/d_p ratios in order to verify the use of plug dispersion models [58,70–72]. Furthermore, criterion Eq. (36) does not take into account the wall effect and therefore, it is not expected to be accurate especially at low d_t/d_p ratios. For low aspect ratios, say $d_t/d_p < 10$, the plug flow assumption fails due to flow non-uniformities [73,74]. On the other hand, using large d_t/d_p ratios (e.g., $d_t/d_p > 10$) to ensure a more uniform profile over a large part of the bed cross section will significantly increase the asymptotic time rates of $D_L(t)$, according to the present model and pore–scale simulation results findings [19,30]. This is doing the opposite to what should be done in ensuring a constant D_L.

In Table 3, we evaluated criteria Eqs. (36) and (39) for some experiments. The order of magnitudes of L/d_t predicted by criterion Eq. (39) are in apparent conflict with those predicted by criterion Eq. (36) for the cases presented in Table 3. For example, Hans criterion Eq. (36) for the experiments in references [45,46] overestimated the L/d_p ratio predicted by the present model especially at large values of Peclet number. Furthermore, Hans criterion underestimated the L/d_t ratios for the experiments in references [60,64]. This apparent conflict in the order of magnitudes of the asymptotic time scales can be mainly attributed to two reasons. First is the error in plotting $D_L(t)$ as a ratio of $D_L(t_i)/D_L(t_5)$; $i = 1$, 2, 3 and 4 where $D_L(t)$ was measured at five different locations along the bed. Without this representation of $D_L(t)$ and under Han's experimental conditions, $D_L(t)$ will not have reached its asymptotic rate in their experiments [19]. Furthermore, the bed dimensions in Hans experiment do not satisfy criterion Eq. (39) proposed in this study as shown in Table 1. This raise serious doubts regarding the applicability of criterion Eq. (36). Second is the possible effect of wall confinement on the asymptotic dispersion rates which was not taken into consideration in ref. [4].

In Table 4 we listed the experimental conditions and the length scales as reported in ref. [19] for a number of random sphere packings in cylinders with different radii. Comparing the length scales (L/d_t ratios without brackets in Table 4) over which the longitudinal dispersion coefficients were evaluated in ref. [19] with those predicted by Eq. (27) clearly reveals the following observations.

- The L/d_t ratios for cylinder packings #7 and #9 satisfy the L/d_t restriction predicted by criterion Eq. (27). It should be noted from Table 4 that the actual L/d_t ratios of the different cylinder packings are larger than the length scales over which the dispersion coefficients were evaluated [19].

Table 1
Some expeiments for evaluating D_L of liquids in packed beds

Reference	Solvent	Solute	Packed bed	ε	d_p (mm)	L (mm)	d_t (mm)	Re	Sc	L/d_t	L/d_t Eq. (39)
Danckwerts [42]	Water	Red dye	Raschig rings	0.62	9.5	1400	48.3	22	1858	28.98	4.48
Kramers and Alberda [43]	Water	NaCl	Raschig rings	0.75	9.5	340	74	75–150	560	4.6	5.06–5.86
Jacques and Vermeulen [44]	Water	$NaNO_3$	Glass spheres	0.26–0.4	5.6-19.1	304.8–640	66.0	5.3–1940	820	4.6–9.69	0.65–5.45
Carberry and Bretton [45]	Water	$NaNO_3$	Glass spheres	0.37–0.65	0.5–6.0	152–914	38.1	1.5–940.2	1858	3.98–23.98	2.06–76.2
Ebach and White [46]	Water	Blue dye	Glass sphere	0.34–0.629	0.21–6.73	1524	50.8	0.02–40	1858	30	2.47–174.5
Strang and Geankopolis [47]	Water	NaCl	Glass sphere	0.411–0.678	6.0–11.6	382–580	41.9	5.0–31.8	894	9.11–13.6	3.87–6.2
Cairns and Prausnitz [48]	Water	KCl	Glass sphere	0.38	1.3–3.2	142–609.6	60.9	3.5–1700	770	2.33–10	12.9–41.89
Liles and Geankopolis [49]	Water	2-Naphtol	Glass sphere	0.36–0.4	0.47–6.13	58.5–1740	50.8	2.4–105	743	1.15–34.25	2.45–98.73
Harrison et al. [50]	Water	Xylene-Cyanol	Glass sphere	0.4[a]	38.1	4877	100	20–100	570	48.77	0.88–1.3
Hiby [51]	Water	NaCl	Glass sphere	0.4[a]	0.5–16	400	90	0.03–70	545	4.44	1.74–63.68
Hennico et al. [52]	Water	$NaNO_3$	Glass sphere	0.4[a]	9.6–19.1	305–60046	63.5	3–300	820	4.8–945	2.0–6.5
Pfannkuch [53]	Water	NaCl	Glass spheres or Sand	0.34–0.39	0.35–2.1	750–1500	75–120	0.00025–3.45	560	6.25–20	2.43–53.05
Miller and King [54]	Water	$NaNO_3$	Glass spheres	0.39	0.051–1.4	140–560	12.7	0.0035–36	730	11–44	1.2–99.37
Smith and Bretton [55]	Water	Blue dye	Glass sphere	0.4[a]	1.0–3.0	304.8–2134	38.1	10–1000	1858	8–56	3.72–24.9
Chung and Wen [56]	Water	$Na_2C_{20}H_{10}O_5$	Glass spheres	0.4	2.0–6.25	810	51	25–320	675	15.88	2.47–11.75
Miyauchi and Kikuchi [57]	Water	NaCl	Glass sphere	0.398	1.48	150–600	20	0.004–13.5	665	7.5–30	1.85–7.78
Han et al. [4]	Water	NaCl	Glass sphere	0.39–0.41	10–15.8	1500	270	0.13–5.2	560	5.55	7.83–3.58
Guedes de Carvalho and Delgado [58]	Water	NaCl	Glass sphere	0.37 0.38	0.625 0.462	3000 700	47 35	0.02–89.1 0.02–34.7	57–754 754–1938	63.829 20	5.33–23.45 22.33–29.6

[a] Assumed value.

Table 2
Some expeiments for evaluating D_L of gases in packed beds

Reference	Solvent	Solute	Packed bed	ε	d_p (mm)	L (mm)	d_t (mm)	Re	Sc	L/d_t	L/d_t Eq. (39)
McHenry and Wilhem [59]	H_2	N_2	Glass Spheres	0.388	3.23	280.4–887	49.58	10.4–379	0.3–1	5.65–17.8	2.08–4.25
Carberry and Bretton [45]	He	Air	Glass Spheres	0.365	6.4	152.4–914.4	25.9	0.015–0.1	0.3	5.88–35.2	0.0015–0.01
Blackwell et al. [60]	Argon	He	Sand	0.339	0.21	36576	161.5	0.0058–0.39	1.9	226	0.71–38.4
DeMaria and White [61]	Air	He	Raschig rings	0.4[a]	6.35–12.7	1422.4	101.6	18.6–198	0.3	14	1.43–4.36
Sinclair and Potter [62]	Hg_{vap}	Air	Glass Sphere	0.4	0.44–1.4	457.2	50.8	1.25–21.1	1.2	9	3.2–29.3
Evans and Kenney [63]	N_2	H_2	Lead shot	0.36–0.374	0.34–2.6	3200	25.9	0.5–10	0.3–0.85	123	0.12–14.9
Edwards and Richardson [64]	Air	Argon	Glass Sphere	0.368–0.42	0.61–4.57	216–1158	82.55	0.008–50	0.72	2.16–14	0.008–32.95
Balla and Weber [65]	CH_4	He	Glass Spheres	0.365	5.0	1045	74	0.031–1.18	2.20	14.12	0.084–1.77
Urban and Gomezplata [66]	He	N_2	Glass Spheres	0.38–0.41	5.95–16.0	1570	101	0.1–150	0.35	15.54	0.018–4.7
Scott et al. [67]	He	N_2	Steel Spheres	0.181–0.556	7.1–15.8	181–1060	9.39–22.03	0.3–100	0.205–1.662	8.21–112	0.003–1.2
Hsiang and Haynes [68]	He	N_2	Glass Sphere	0.4–0.66	2.1–15.2	1530	3.9–17.2	4–500	0.22	88.95–392	0.015–0.506
Benneker et al. [69]	N_2	He (SF)	Glass Spheres	0.4	2.2–3.9	3000	25–50	5–250	0.23	60–120	0.46–3.08
Yu et al. [70]	CH_4	CO_2 (SF)	Sand	0.33–0.41	0.097–0.16	50	4.6	0.004–1.2	2–9	10.86	0.019–8.94

[a] Assumed value.

Table 3
Comparison between criteria Eqs. (36) and (39) for some experimental conditions for evaluating D_L of liqiuds and gases in packed beds

Reference	Solvent	Solute	Packed Bed	ε	d_p (mm)	L (mm)	d_t (mm)	Re	Sc	$Pe_p\ \varepsilon/(1-\varepsilon)$ [4]	L/d_t	L/d_t Eq. (36)	L/d_t Eq. (39)
Edwards and Richardson [64]	Air	Argon	Glass Sphere	0.368–0.41	0.61–4.57	216–1158	82.55	0.008–50	0.72	0.0053–50.1	2.16–14	0.000012–0.83	0.008–32.95
Carberry and Bretton [45]	Water	$NaNO_3$	Glass Spheres	0.37–0.65	0.5–6.0	152–914	38.1	1.5–940.2	1858	276–7.24 E + 06	3.98–23.98	1.08–2.85E + 05	2.06–76.2
Ebach and White [46]	Water	Blue dye	Glass Sphere	0.34–0.629	0.21–6.73	1524	50.8	0.02–40	1858	26.3–3.26 E + 06	30	0.033–1.29 E + 05	2.47–174.5
Pfannkuch [53]	Water	NaCl	Glass Spheres or Sand	0.34–0.39	0.35–2.1	750–1500	75–120	0.00025–3.45	560	0.199–3405	6.25–20	0.00017–28.602	2.43–53.05
Blackwell et al. [60]	Argon	He	Sand	0.339	0.21	36576	161.5	0.0058–0.39	1.9	0.0028–0.188	226	1.09 E-06–7.33 E-05	0.71–38.4

Table 4
Comparison of the length scales used for the pore–scale simulation of Maier et al. [19] and those obtained from criterion Eq. (27)

Cylinder #	R	L	$\bar{\varepsilon}$	L/d_t [19]	L/d_t Eq. (27)
1	$6.5d_p$	$48.6d_p$	0.407	1.5 (3.74)	27.7
2	$12.5d_p$	$50.5d_p$	0.400	0.8 (2.02)	53.2
3	$25d_p$	$53.7d_p$	0.400	0.4 (1.07)	106
4	$6d_p$	$486d_p$	0.410	16 (41)	25.5
5	$12d_p$	$524d_p$	0.410	8.4 (21.8)	51
6	$24d_p$	$547d_p$	0.410	4.2 (11.5)	102
7	$5d_p$	$1172d_p$	0.400	20 (117.2)	21.3
8	$24d_p$	$47.7d_p$	0.399	0.42 (≈1.0)	100
9	$4.78d_p$	$955d_p$	0.400	20	20

Values of L are based on the mean displacement. Values within brackets are the physical L/d_t ratios for different cylinder packings. [$d_p = 3$ mm, $D_m = 2.1 \times 10^{-9}$ m^2/s, $\nu = 1.1 \times 10^{-6}$ m^2/s, $\hat{D}_T/D_m = 15$, ($\hat{D}_L/D_m = 224$ for #1, 2, 3 and 8; $\hat{D}_L/D_m = 200$ for #4, 5 and 6; $\hat{D}_L/D_m = 232$ for #7 and 9), $R_{ep} = \bar{u}d_p/\nu = 1.0$, $P_{em} = \bar{u}d_p/D_m = 476$].

- The length scale over which the longitudinal dispersion coefficients for cylinder packing #4 were obtained is not as close to that predicted by criterion Eq. (27) as the case for cylinder packings #7 and #9. This is confirmed by the long time predictions using pore–scale simulation which shows that the asymptotic dispersion rates were only obtained with the cylinder packings #7 and #9 and closely reached with cylinder packing #4 within the available simulation time [19].

However, using pore–scale simulation for long time analysis (i.e., $t \gg 20d_p/\bar{u}$) for beds of intermediate to large lengths, is not expected to give an accurate estimate of the asymptotic dispersion values [19]. For example, increasing the spatial resolution, say from $d_p/25$ to $d_p/8$, will lead to an error in evaluating the magnitude of the velocity maximum near the wall [19]. This led to underestimated values of $D_L(t)$ when compared with the higher resolution results. However, improving the accuracy by using higher spatial resolution is totally limited by the computational memory available. Because of that, the Taylor–Aris model was used in ref. [19] to predict the qualitative behaviour of $D_L(t)$ in the case of long cylinders.

The NMR results for $R = 10d_p$ show that the asymptotic dispersion rates are less than those predicted by criterion Eq. (34) [23]. This is expected as the results in reference [23] do not account for the possible effect of the wall confinement [19]. Therefore, the asymptotic rates were obtained on a convective time scale proportional $d_p/\bar{u}$ [19,23,30], as in the case for unconfined packings. This time scale is within the limits of NMR techniques and is less than the asymptotic scale proportional to $R^2/\langle D_T \rangle$.

4. Case study

Our case study is restricted to the dispersion of a solute into a fluid flowing through a porous medium where the flow obeys the Darcy model. It is possible to analyse the pulses of C with time in a convenient fashion by calculating the moments of the $\bar{C}$ distribution to evaluate the essential distribution features (e.g., the distribution mean μ_1, variance μ_2, skewness Γ and kurtosis Δ) as shown in Appendix D.

The functions of $D_L(\theta)/D_L(\infty)$ and $V(\theta)/V(\infty)$ for the case study are given in Appendix D and shown in Fig. 2 while the functions of variance, skewness and kurtosis (see Appendix D) are shown in Fig. 3a and b. As shown in Fig. 2, the effective axial dispersion coefficient $D_L(\theta)$ approaches its asymptotic rate at large times. However, other persisting transients accompanying the dispersion process may take longer times to reach their asymptotic rates as shown in the graph of $V(\theta)/V(\infty)$ in Fig. 2. For example, to reach 60% of the asymptotic $D_L(\infty)$ and $V(\infty)$ values, mean dispersion lengths of $0.23R$ times $D_L(\infty)$ and of $1.5R$ times $V(\infty)$ are needed,

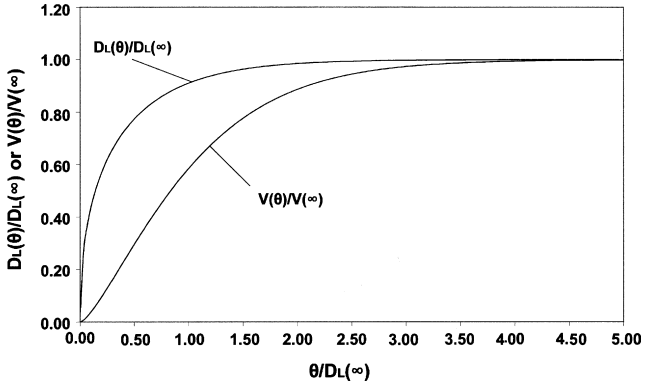

Fig. 2. The functions of $D_L(\theta)/D_L(\infty)$and $V(\theta)/V(\infty)$ at $Pe_{Rm} = Pe_{Lm} = 20$ and for various values of $\theta/D_L(\infty)$.

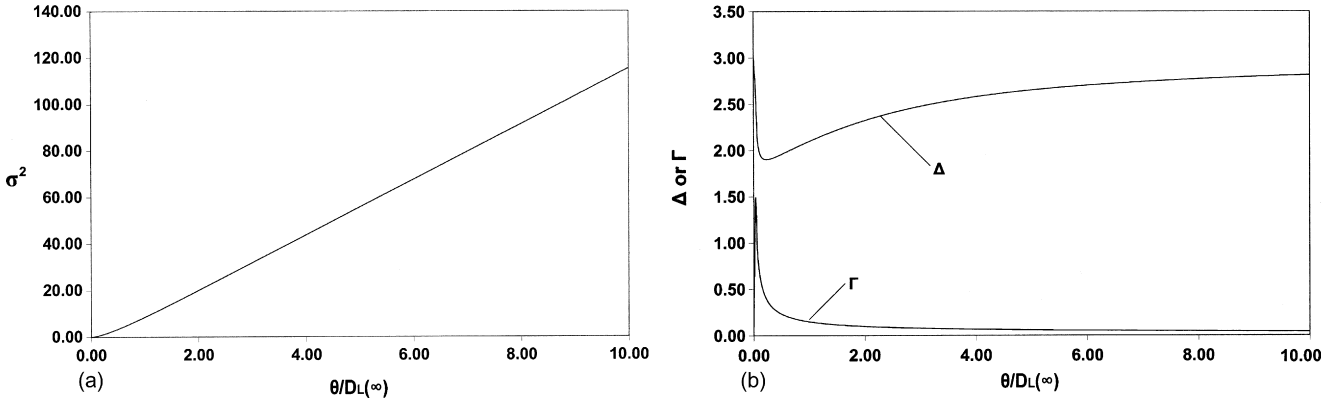

Fig. 3. The moments of distribution at $Pe_{Rm} = Pe_{Lm} = 20$ and for various values of $\theta/D_L(\infty)$. (a) Variance, σ^2; (b) skewness, Γ, and kurtosis, Δ.

respectively. To achieve 90% of the asymptotic $D_L(\infty)$ and $V(\infty)$ values, mean dispersion lengths over $0.95R$ times $D_L(\infty)$ and of $2.1R$ times $V(\infty)$ are needed, respectively. Therefore, analysing dispersion data when working with laboratory scales less than the asymptotic time scales is not possible using the classical plug dispersion model due to the dispersion transients that can persist further downstream. This point can also be clarified if we consider a concentration distribution with μ_2 at a point, say $0.36RD_L(\infty)$ (or equivalently $\theta = 0.88$ or $\theta/D_L(\infty) = 0.36$). Based on the plug dispersion model, the asymptotic longitudinal dispersion coefficient $D_L(\infty)$ can be evaluated from the second moment [4,31].

$$D_L(\infty) = \frac{\mu_2}{2\theta} \tag{40}$$

From Fig. 2 and at $\theta/D_L(\infty) = 0.36$, the value of $D_L(\theta)$ is approximately 0.7 times $D_L(\infty)$. At the same $\theta/D_L(\infty)$ value, Fig. 3a gives $\mu_2 \cong 2.2$ (or $\mu_2/2\theta \cong 1.25$) which is approximately 51% of the asymptotic $D_L(\infty)$. Therefore, at this time scale, the plug dispersion model (Eq. (40)) tends to underestimate the actual dispersion coefficient values in both cases by 30% and 49%, respectively.

Due to the spread of the pulse, the second moment of distribution is always an increasing function in θ (Fig. 3a) and at large times it increases linearly with time ($D_L(\theta)/D_L(\infty) \to 1$) as the case in the plug (Fickian) dispersion models. After a time $\theta/D_L(\infty) \approx 2$, μ_2 follows a straight line and the slope of the line is proportional to the asymptotical dispersion coefficient $D_L(\infty)$. As shown in Fig. 2 and at short to intermediate time scales, the pulse spreads at a faster rate than at larger times ($\theta \to \infty$) where the pulse width is proportional to the square root of time. According to Eq. (D.12), the second moment is only affected by the second derivative term in the averaged transport Eq. (16).

Fig. 3b shows that the skewness of the pulse, Γ, will decay at a much faster rate than the kurtosis effect, Δ, and larger dispersion distances are needed for Δ to attain its asymptotic value. This is clarified by the equations in Appendix D which describe Γ and Δ as a function of time. For large times, Γ will decrease as $\theta^{-1/2}$ while Δ will approach the limiting value of 3 as θ^{-1} (Fig. 3b). These findings are in accordance with the observations for the case of solute dispersion in empty tubes [77]. Evaluating the higher order moments Γ and Δ as a function of time provides a very important tool to study how the concentration distribution approaches Gaussinity. For example, at time $\theta = 4D_L(\infty)$, $\Delta(\theta)$ is 90% of the asymptotic value $\Delta(\infty) = 3$ while $\Gamma(\theta)$ is very small and approaches the asymptotic zero value much faster than $\Delta(\theta)$. At this time scale, the concentration profile may approach the normal Gaussian distribution.

In porous media, the mass transport transverse to the flow direction is less than the mass transport in the flow direction and at very low flow velocities, it is expected that the rate of transport in both directions will be of the same order of magnitude [78]. The effect of varying the flow Peclet numbers Pe_{Lm} and Pe_{Rm} on $D_L(\theta)$ and $V(\theta)$ is shown in Fig. 4a and b. The temporal behaviour of $D_L(\theta)$ and $V(\theta)$ is dependent on the negative power of the exponent terms (i.e., θ/P_{Rm}) and for larger values of Pe_{Rm}, one needs larger dispersion times in order to treat D_L and V as constants (i.e., $D_L(\theta)/D_L(\infty) \to 1$; $V(\theta)/V(\infty) \to 1$). The negative power of the exponent function, $\lambda\theta$ or equivalently $t\langle D_T\rangle/R^2$, shows that the time scale to reach the asymptotic behaviour of $D_L(\theta)$ and $V(\theta)$ is controlled by the bed radius and $\langle D_T\rangle$. The asymptotic time scales of $D_L(\theta)$ and $V(\theta)$ depend on the behaviour of the exponent functions in Eqs. (18) and (19). The difference between the two functions $(1 - e^{-\lambda\theta})$ and $(1 - \lambda\theta)e^{-\lambda\theta}$ is approximately of the form $\lambda\theta\, e^{-\lambda\theta}$. Therefore, as Pe_{Rm} is increased (i.e, R increases and/or $\langle D_T\rangle$ decreases), the difference between the two asymptotic time scales to attain $D_L(\infty)$ and $V(\infty)$ becomes larger as shown in Fig. 4a.

The pulse spread around the mean, μ_2, increases significantly with the increase in the Peclet number Pe_{Rm}, Fig. 4b. This is in accordance with the solute dispersion findings in empty tubes where Taylor dispersion effect was found to be proportional to the mean flow velocity, tube radius and inversely proportinal to the solute diffusion coefficient [5]. The time needed for μ_2 to reach the linear part of the curve μ_2 versus θ (Fickian behaviour) becomes larger as Pe_{Rm} is assigned higher values. This is clearly shown by Eq. (D.12) where for high values of Pe_{Rm} the negative exponent term will approach zero at a slower rate than at lower Pe_{Rm} values.

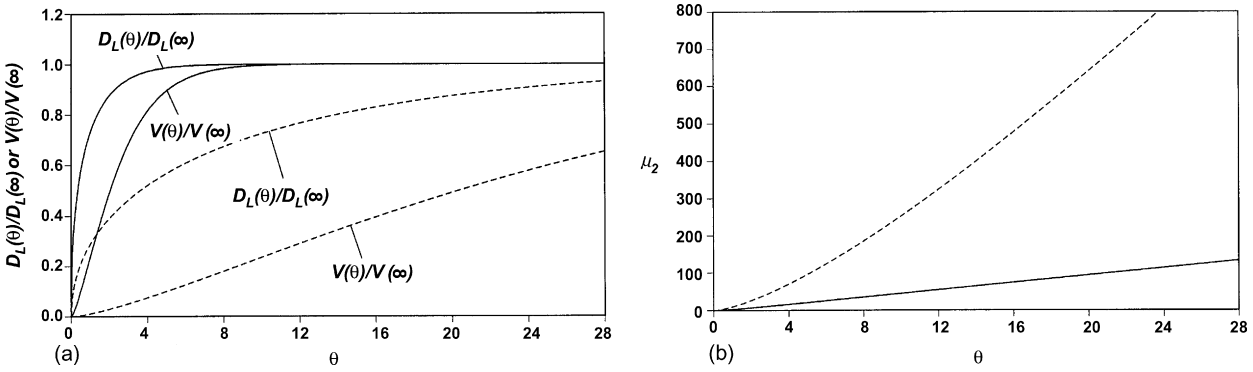

Fig. 4. The effect of the flow parameter Pe_{Rm} on the temporal behaviour of $D_L(\theta)$ and μ_2. (a) $D_L(\theta)/D_L(\infty)$; (b) Variance, μ_2, for (—) $Pe_{Rm} = Pe_{Lm} = 20$, (- - -) $Pe_{Rm} = 200$ and $Pe_{Lm} = 20$.

The results show that decreasing the transverse spreading or increasing the bed radius will require larger time scales to reach $D_L(\infty)$ and $V(\infty)$.

The expressions for the moments of distribution given in Appendix D, show that the time scales for attaining the asymptotic $\Gamma(\infty)$ and $\Delta(\infty)$ are dependent on the ratio θ/Pe_{Rm}. Changing Pe_{Rm} have an opposite effect on the temporal behaviour of $\Gamma(\theta)$ and $\Delta(\theta)$ as shown in Fig. 5a. While increasing Pe_{Rm} increases the asymptotic time scale for $\Delta(\theta)$, it reduces the asymptotic time scale for $\Gamma(\theta)$. The same results can be reached by careful inspection of the variation of the $\Gamma(\theta)$ and $\Delta(\theta)$ functions in Appendix D with Pe_{Rm}. Therefore, assigning high values of Pe_{Rm} will require larger times for $\Delta(\theta)$ and less times for $\Gamma(\theta)$ to attain their ultimate values. The dependency of $\Delta(\theta)$ on θ/Pe_{Rm} can only be studied numerically because of the difficulty in evaluating analytically the term $\int_0^\theta K_0(\theta)K_3(\theta)\,d\theta$. To investigate the dependency of the two terms, $\int_0^\theta K_0(\theta)K_3(\theta)\,d\theta$ and $\int_0^\theta K_4(\theta)\,d\theta$ in the $\Delta(\theta)$ equation in Appendix D, we define

$$\hat{H}(\theta) = \frac{24}{\mu_2^2}\int_0^\theta K_4(\theta)\,d\theta \tag{41}$$

and

$$\hat{S}(\theta) = \frac{24}{\mu_2^2}\int_0^\theta K_0(\theta)K_3(\theta)\,d\theta \tag{42}$$

The results of numerical integration of the terms $\hat{H}(\theta)$ and $\hat{S}(\theta)$ are shown in Fig. 5b. In general, $\hat{H}(\theta)$ approaches its ultimate zero value at a much faster rate than $\hat{S}(\theta)$. The effect of $\hat{H}(\theta)$ is only significant at the early stages of dispersion and its contribution to the pulse peakedness becomes less significant at larger Pe_{Rm} values. In this case, the $\Delta(\theta)$ function in Eq. (D.16) can be approximated as

$$\Delta(\theta) \cong 3 + \frac{24}{\mu_2^2}\int_0^\theta K_0(\theta)K_3(\theta)\,d\theta \tag{43}$$

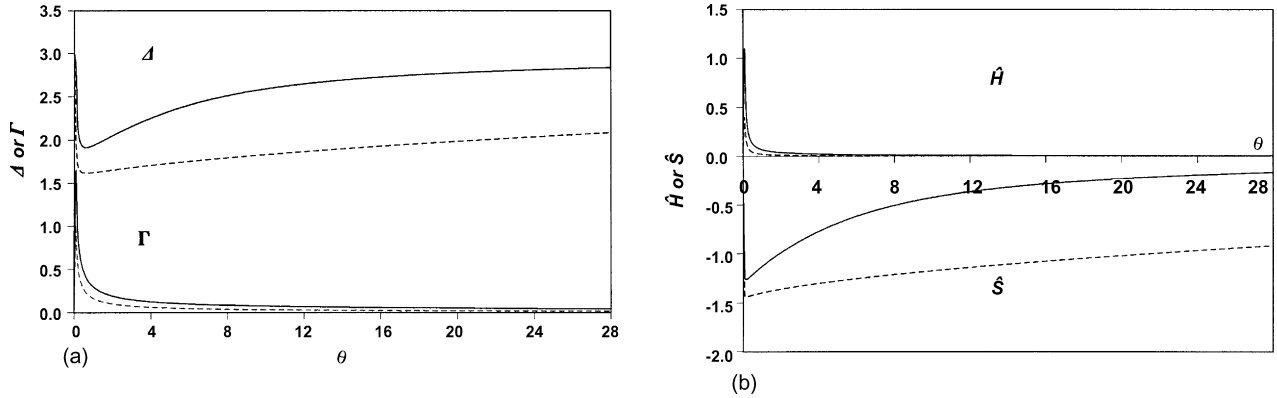

Fig. 5. The effect of the flow parameter Pe_{Rm} on the temporal behaviour of $\Delta(\theta)$, $\Gamma(\theta)$, $\hat{H}(\theta)$ and $\hat{S}(\theta)$. (a) $\Delta(\theta)$ and $\Gamma(\theta)$; (b) $\hat{H}(\theta)$ and $\hat{S}(\theta)$, for (—) $Pe_{Rm} = Pe_{Lm} = 20$, (- - -) $Pe_{Rm} = 200$ and $Pe_{Lm} = 20$.

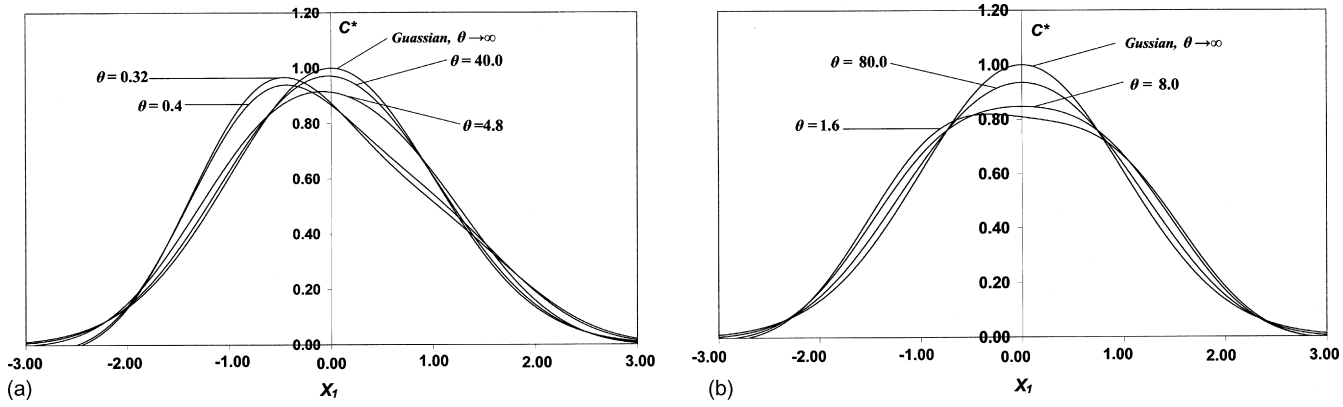

Fig. 6. The concentration profile distribution, $C^* = \left(\sqrt{2\pi\mu_2}/\mu_0\right)\bar{C}$, vs. x_1 at various values of θ. (a) $Pe_{Rm} = Pe_{Lm} = 20$; (b) $Pe_{Rm} = Pe_{Lm} = 200$.

Under such conditions, the contribution of the dispersion term $\partial^4\bar{C}/\partial x^4$ may be neglected and the average macroscopic transport Eq. (16) can be approximated by setting $K_4(\theta) \cong 0$.

The contribution of the $\hat{S}(\theta)$ controls the pulse peakedness and its effect is expected to persist for larger distances from the injection point. The asymptotic time scale for $\hat{S}(\theta)$ to reach $\hat{S}(\infty)$ is proportional to Pe_{Rm} (Fig. 5b). Therefore, at larger Pe_{Rm} values, $\hat{S}(\theta)$ requires longer dispersion times than $\hat{H}(\theta)$ to attain their long time behaviour.

4.1. Expression of $\bar{C}$ by an edgeworth series

The observed non-Guassian profiles of $\bar{C}$ can be presented using the Edgeworth form of the Graham Charlier series type A [79]. The three term Edgeworth series for the non-Gaussian distribution can be expressed as [79].

$$\frac{\sqrt{2\pi\mu_2}}{\mu_0}\bar{C} = \exp\left(-\frac{\tau^2}{2}\right)\left[1 + \frac{\lambda_3}{6}H_3(\tau) + \frac{\lambda_4}{24}H_4(\tau) + \frac{\lambda_3^2}{72}H_6(\tau)\right] \tag{44}$$

The definition of the different terms of the series is shown in Appendix E. The solution of Eq. (16) could be approximated by the expansion in Eq. (44). The spatial distribution of $C^* = \left(\sqrt{2\pi\mu_2}/M_0\right)\bar{C}$ versus x_1 at various θ times during the dispersion process is shown in Fig. 6a and b for $Pe_{Rm} = 20$ and 200, respectively. At relatively small times in the dispersion process and provided that Pe_{Rm} is sufficiently small, the concentration profile could be skewed from the normal distribution as shown in Fig. 6a. Later in the dispersion process, the skewness of the pulse dies out rapidly and the distribution becomes nearly symmetric but the kurtosis effect may persist further downstream and the distribution profile could become slightly flattened. Increasing the flow Peclet number Pe_{Rm} reduces the skewness of the pulse as shown in Figs. 5b and 6b. However, the peakedness of the pulse is proportional to Pe_{Rm} as shown by $\hat{S}(\theta)$ function in Fig. 5b. Therefore, the mean concentration $\bar{C}$ at higher values of Pe_{Rm} (Fig. 6b) exhibits more pulse flatness and less skewness than at lower Pe_{Rm} values (Fig. 6a). The flatness of the profile is merely due to the kurtosis effect as a result of the dispersive terms $\partial^3\bar{C}/(\partial x_1^2\partial\theta)$ and $\partial^4\bar{C}/\partial x_1^4$ where the contribution of the dispersion term $\partial^3\bar{C}/(\partial x_1^2\partial\theta)$ to the pulse peakedness is much more significant than $\partial^4\bar{C}/\partial x_1^4$ at sufficiently large Pe_{Rm} as shown from the behaviour of $\hat{H}(\theta)$ and $\hat{S}(\theta)$ in Fig. 5b.

5. Conclusion

An extended axial non-Fickian macroscopic dispersion model has been developed which provides a more detailed description of the dispersion process than the existing plug flow dispersion models. The significance of this model is the inclusion of higher order, time-dependent dispersion terms and most importantly, the dispersion term $\partial^3\bar{C}/(\partial x_1^2\partial\theta)$. It was found that this term affects the peakedness of the distribution and may persist for long times after the introduction of the solute and causes the deviation from Gaussinity. The extended model allows evaluating the moments of the distribution as functions of time, thus providing a measure for the degree of deviation from Gaussinity as the dispersion time increases. This is very important because it provides an estimate of the dispersion lengths (i.e., equipment dimension) required for attaining time-independent, non-Fickian transients and hence, specifies the range of applicability of the conventional plug dispersion models. Pore–scale simulation and the extended model results show that the time scale for $D_L(t)$ to attain the asymptotic dispersion rates is proportional to $R^2/\langle D_T\rangle$ and not dependent on the convective nor diffusive time scales. Model analysis suggests that D_L is not constant unless the approximate criterion $\theta^* \geq 0.264$ is satisfied. Furthermore, increasing the bed radius and/or decreasing the transverse spreading causes the effect of the dispersion term $\partial^3\bar{C}/(\partial x_1^2\partial\theta)$ to persist for larger dispersion distances and therefore, the tracer experiment has to be conducted over longer times to minimise its effect. The results also show that increasing R as a means to obtain a nearly uniform flow profile over the majority of

the bed cross section as done by many researchers, will significantly affect the range of applicability of the plug dispersion model. This is due to the square dependence of the asymptotic time scales on R.

Appendix A

Using the integral transform pair

$$\bar{T} = \int_0^1 \zeta J_0(\beta_m, \zeta)\tilde{C}\,\mathrm{d}\zeta \tag{A.1}$$

$$\tilde{C} = \sum_{m=1}^{\infty} \frac{J_0(\beta_m, \zeta)}{N(\beta_m)}\bar{T} \tag{A.2}$$

the integral transform of Eq. (14) is

$$\frac{\partial \bar{T}}{\partial \theta} + \lambda \bar{T} - \frac{1}{Pe_{\mathrm{Lm}}}\frac{\partial^2 \bar{T}}{\partial x_1^2} = \bar{g}(x_1, \theta, \zeta); \tag{A.3}$$

$$\lambda = \frac{1}{Pe_{\mathrm{Rm}}}(\beta_m)^2, \quad \bar{g}(x_1, \theta) = -\frac{1}{\bar{\varepsilon}}\frac{\partial \bar{C}}{\partial x_1}\int_0^1 \zeta J_0(\beta_m, \zeta)\tilde{u}\,\mathrm{d}\zeta + \frac{1}{Pe_{\mathrm{Lm}}}\frac{\partial^2 \bar{C}}{\partial x_1^2}\int_0^1 \zeta J_0(\beta_m, \zeta)\tilde{D}_{\mathrm{A}}^*\,\mathrm{d}\zeta + \frac{1}{\bar{\varepsilon}Pe_{\mathrm{Lm}}}\frac{\partial^2 \bar{C}}{\partial x_1^2}\int_0^1 \zeta J_0(\beta_m, \zeta)\tilde{\varepsilon}\,\mathrm{d}\zeta \tag{A.4}$$

The solution of Eq. (A.3) is given by [35]

$$\bar{T} = \int_{t'=0}^{\theta}\int_{\omega=-\infty}^{\infty} \frac{\bar{g}(x_1, \theta, \zeta)}{[4\pi(\theta - t')/Pe_{\mathrm{Lm}}]^{1/2}}\exp(\lambda\theta)\exp\left[-Pe_{\mathrm{Lm}}\frac{(x_1 - w)^2}{4(\theta - t')}\right]\mathrm{d}w\,\mathrm{d}t' \tag{A.5}$$

Following [10], the integral can be approximated by expanding $\bar{g}(x_1, \theta, \zeta)$ around $w = x_1$ and $t = \theta$ and retaining only first order terms in $(w - x_1)$ and $(t - \theta)$ to yield

$$\bar{T} = \bar{g}\left(\frac{1 - \mathrm{e}^{-\lambda\theta}}{\lambda}\right) - \left(\frac{\partial \bar{g}}{\partial \theta} - \frac{1}{Pe_{\mathrm{Lm}}}\frac{\partial^2 \bar{g}}{\partial x_1^2}\right)\left(\frac{1 - (1 + \lambda\theta)\,\mathrm{e}^{-\lambda\theta}}{\lambda^2}\right) \tag{A.6}$$

Using Eq. (A.2), one can find

$$(\overline{\tilde{u}\tilde{C}}) = \sum_{m=1}^{\infty} \frac{\overline{\tilde{u}\,J_0(\beta_m, \zeta)}}{N(\beta_m)}\bar{T} \tag{A.7}$$

$$(\overline{\tilde{\varepsilon}\tilde{C}}) = \sum_{m=1}^{\infty} \frac{\overline{\tilde{\varepsilon}\,J_0(\beta_m, \zeta)}}{N(\beta_m)}\bar{T} \tag{A.8}$$

$$\overline{(\tilde{D}_{\mathrm{A}}^*\tilde{C})} = \sum_{m=1}^{\infty} \frac{\overline{\tilde{D}_{\mathrm{A}}^* J_0(\beta_m, \zeta)}}{N(\beta_m)}\bar{T} \tag{A.9}$$

Substituting Eqs. (A.7)–(A.9) into Eq. (11) yields Eq. (16).

Appendix B

$$\frac{\partial \bar{C}}{\partial \theta} = K_0(\theta)\frac{\partial^2 \bar{C}}{\partial x_1^2} + K_1(\theta)\frac{\partial^2 \bar{C}}{\partial x_1 \partial \theta} + K_2(\theta)\frac{\partial^3 \bar{C}}{\partial x_1^3} + K_3(\theta)\frac{\partial^3 \bar{C}}{\partial x_1^2 \partial \theta} + K_4(\theta)\frac{\partial^4 \bar{C}}{\partial x_1^4} + K_5(\theta)\frac{\partial^4 \bar{C}}{\partial x_1^3 \partial \theta} \tag{B.1}$$

where

$$K_0(\theta) = -\sum_{m=1}^{\infty} \frac{\overline{\tilde{u}\,J_0(\beta_m, \zeta)}}{\bar{\varepsilon}N(\beta_m)}\left(\frac{1 - \mathrm{e}^{-\lambda\theta}}{\lambda}\right)A_0 + \frac{1}{Pe_{\mathrm{Lm}}} + \frac{\overline{\tilde{D}_{\mathrm{A}}^*\tilde{\varepsilon}}}{\bar{\varepsilon}Pe_{\mathrm{Lm}}} - \sum_{m=1}^{\infty} \frac{\overline{\tilde{\varepsilon}\,J_0(\beta_m, \zeta)}}{\bar{\varepsilon}N(\beta_m)}\mathrm{e}^{-\lambda\theta}B_0 \tag{B.2}$$

$$K_1(\theta) = -\sum_{m=1}^{\infty} \frac{\overline{\tilde{\varepsilon} J_0(\beta_m, \zeta)}}{2\bar{\varepsilon} N(\beta_m)} \left(\frac{1 - \mathrm{e}^{-\lambda\theta}}{\lambda} \right) A_0 + \sum_{m=1}^{\infty} \frac{\overline{\tilde{\varepsilon} J_0(\beta_m, \zeta)}}{\bar{\varepsilon} N(\beta_m)} \theta \, \mathrm{e}^{-\lambda\theta} A_0 - \sum_{m=1}^{\infty} \frac{\overline{\tilde{u} J_0(\beta_m, \zeta)}}{2\bar{\varepsilon} N(\beta_m)} \left(\frac{1 - \mathrm{e}^{-\lambda\theta}}{\lambda} \right) E_0 \tag{B.3}$$

$$K_2(\theta) = \frac{1}{Pe_{\mathrm{Lm}}} \left(\sum_{m=1}^{\infty} \frac{\overline{\tilde{D}_{\mathrm{A}}^* J_0(\beta_m, \zeta)}}{N(\beta_m)} \left(\frac{1 - \mathrm{e}^{-\lambda\theta}}{\lambda} \right) A_0 + \frac{1}{\bar{\varepsilon}} \sum_{m=1}^{\infty} \frac{\overline{\tilde{\varepsilon} J_0(\beta_m, \zeta)}}{N(\beta_m)} \left(\frac{1 - \mathrm{e}^{-\lambda\theta}}{\lambda} \right) A_0 - \frac{1}{\bar{\varepsilon}} \sum_{m=1}^{\infty} \frac{\overline{\tilde{\varepsilon} J_0(\beta_m, \zeta)}}{N(\beta_m)} \theta \, \mathrm{e}^{-\lambda\theta} A_0 \right.$$
$$\left. - \sum_{m=1}^{\infty} \frac{\overline{\tilde{u} J_0(\beta_m, \zeta)}}{\bar{\varepsilon} N(\beta_m)} \left(\frac{1 - \mathrm{e}^{-\lambda\theta}}{\lambda} \right) B_0 \right) \tag{B.4}$$

$$K_3(\theta) = -\sum_{m=1}^{\infty} \frac{\overline{\tilde{\varepsilon} J_0(\beta_m, \zeta)}}{\bar{\varepsilon} N(\beta_m)} \left(\frac{1 - \mathrm{e}^{-\lambda\theta}}{\lambda} \right) B_0 + \sum_{m=1}^{\infty} \frac{\overline{\tilde{\varepsilon} J_0(\beta_m, \zeta)}}{\bar{\varepsilon} N(\beta_m)} \theta \, \mathrm{e}^{-\lambda\theta} B_0 - \sum_{m=1}^{\infty} \frac{\overline{\tilde{u} J_0(\beta_m, \zeta)}}{\bar{\varepsilon} N(\beta_m)} \left(\frac{1 - (1 + \lambda\theta)\mathrm{e}^{-\lambda\theta}}{\lambda^2} \right) A_0 \tag{B.5}$$

$$K_4(\theta) = \frac{1}{Pe_{\mathrm{Lm}}} \left(-\sum_{m=1}^{\infty} \frac{\overline{\tilde{u} J_0(\beta_m, \zeta)}}{\bar{\varepsilon} N(\beta_m)} \left(\frac{1 - (1 + \lambda\theta)\mathrm{e}^{-\lambda\theta}}{\lambda^2} \right) A_0 + \frac{1}{\bar{\varepsilon}} \sum_{m=1}^{\infty} \frac{\overline{\tilde{\varepsilon} J_0(\beta_m, \zeta)}}{N(\beta_m)} \left(\frac{1 - \mathrm{e}^{-\lambda\theta}}{\lambda} \right) B_0 \right.$$
$$\left. + \sum_{m=1}^{\infty} \frac{\overline{\tilde{D}_{\mathrm{A}}^* J_0(\beta_m, \zeta)}}{N(\beta_m)} \left(\frac{1 - \mathrm{e}^{-\lambda\theta}}{\lambda} \right) B_0 - \frac{1}{\bar{\varepsilon}} \sum_{m=1}^{\infty} \frac{\overline{\tilde{\varepsilon} J_0(\beta_m, \zeta)}}{N(\beta_m)} \theta \, \mathrm{e}^{-\lambda\theta} B_0 \right) \tag{B.6}$$

$$K_5(\theta) = -\frac{2}{Pe_{\mathrm{Lm}}} \sum_{m=1}^{\infty} \frac{\overline{\tilde{D}_{\mathrm{A}}^* J_0(\beta_m, \zeta)}}{N(\beta_m)} \left(\frac{1 - (1 + \lambda\theta)\, \mathrm{e}^{-\lambda\theta}}{\lambda^2} \right) A_0 - \frac{3}{\bar{\varepsilon} Pe_{\mathrm{Lm}}} \sum_{m=1}^{\infty} \frac{\overline{\tilde{\varepsilon} J_0(\beta_m, \zeta)}}{N(\beta_m)} \left(\frac{1 - (1 + \lambda\theta)\, \mathrm{e}^{-\lambda\theta}}{\lambda^2} \right) A_0 \tag{B.7}$$

At large times,

$$K_0(\infty) = -\sum_{m=1}^{\infty} \frac{\overline{\tilde{u} J_0(\beta_m, \zeta)}}{\lambda\bar{\varepsilon} N(\beta_m)} A_0 + \frac{1}{Pe_{\mathrm{Lm}}} + \frac{\overline{\tilde{D}_{\mathrm{A}}^* \tilde{\varepsilon}}}{\bar{\varepsilon} Pe_{\mathrm{Lm}}} \tag{B.8}$$

$$K_1(\infty) = -\sum_{m=1}^{\infty} \frac{\overline{\tilde{\varepsilon} J_0(\beta_m, \zeta)}}{2\lambda\bar{\varepsilon} N(\beta_m)} A_0 - \sum_{m=1}^{\infty} \frac{\overline{\tilde{u} J_0(\beta_m, \zeta)}}{2\lambda\bar{\varepsilon} N(\beta_m)} E_0 \tag{B.9}$$

$$K_2(\infty) = \frac{1}{Pe_{\mathrm{Lm}}} \left(\sum_{m=1}^{\infty} \frac{\overline{\tilde{D}_{\mathrm{A}}^* J_0(\beta_m, \zeta)}}{\lambda N(\beta_m)} A_0 + \frac{1}{\bar{\varepsilon}} \sum_{m=1}^{\infty} \frac{\overline{\tilde{\varepsilon} J_0(\beta_m, \zeta)}}{\lambda N(\beta_m)} A_0 - \sum_{m=1}^{\infty} \frac{\overline{\tilde{u} J_0(\beta_m, \zeta)}}{\lambda\bar{\varepsilon} N(\beta_m)} B_0 \right) \tag{B.10}$$

$$K_3(\infty) = -\sum_{m=1}^{\infty} \frac{\overline{\tilde{\varepsilon} J_0(\beta_m, \zeta)}}{\lambda\bar{\varepsilon} N(\beta_m)} B_0 - \sum_{m=1}^{\infty} \frac{\overline{\tilde{u} J_0(\beta_m, \zeta)}}{\lambda^2\bar{\varepsilon} N(\beta_m)} A_0 \tag{B.11}$$

$$K_4(\infty) = \frac{1}{Pe_{\mathrm{Lm}}} \left(-\sum_{m=1}^{\infty} \frac{\overline{\tilde{u} J_0(\beta_m, \zeta)}}{\lambda^2\bar{\varepsilon} N(\beta_m)} A_0 + \frac{1}{\bar{\varepsilon}} \sum_{m=1}^{\infty} \frac{\overline{\tilde{\varepsilon} J_0(\beta_m, \zeta)}}{\lambda N(\beta_m)} B_0 + \sum_{m=1}^{\infty} \frac{\overline{\tilde{D}_{\mathrm{A}}^* J_0(\beta_m, \zeta)}}{\lambda N(\beta_m)} B_0 \right) \tag{B.12}$$

$$K_5(\infty) = -\frac{2}{Pe_{\mathrm{Lm}}} \sum_{m=1}^{\infty} \frac{\overline{\tilde{D}_{\mathrm{A}}^* J_0(\beta_m, \zeta)}}{\lambda^2 N(\beta_m)} A_0 - \frac{3}{\bar{\varepsilon} Pe_{\mathrm{Lm}}} \sum_{m=1}^{\infty} \frac{\overline{\tilde{\varepsilon} J_0(\beta_m, \zeta)}}{\lambda^2 N(\beta_m)} A_0 \tag{B.13}$$

where

$$A_0 = -\frac{1}{\bar{\varepsilon}} \int_0^1 \zeta J_0(\beta_m, \zeta) \tilde{u} \, \mathrm{d}\zeta \tag{B.14}$$

$$B_0 = \frac{1}{Pe_{\mathrm{Lm}}}\left[-E_0 + \int_0^1 \zeta J_0(\beta_m, \zeta)\tilde{D}_{\mathrm{A}}^* \,\mathrm{d}\zeta\right] \tag{B.15}$$

$$E_0 = -\frac{1}{\bar{\varepsilon}}\int_0^1 \zeta J_0(\beta_m, \zeta)\tilde{\varepsilon}\,\mathrm{d}\zeta \tag{B.16}$$

Appendix C

By substituting for λ from (A.4) and D_{L} from (D.3) into Eqs. (30)–(33), the approximate criteria in terms of Pe_{Rm} and Pe_{Lm} are

$$\frac{Pe_{\mathrm{Lm}} + (1/Pe_{\mathrm{Rm}})}{2\alpha_{\mathrm{L}}} L^* \gg 1 \tag{C.1}$$

$$\frac{Pe_{\mathrm{Lm}} + 1/Pe_{\mathrm{Rm}}}{Pe_{\mathrm{Rm}} + \alpha_{\mathrm{L}}^2} L^{*2} \gg 1 \tag{C.2}$$

$$\left(\frac{1}{Pe_{\mathrm{Rm}}} + \frac{1}{Pe_{\mathrm{Lm}} Pe_{\mathrm{Rm}}^2}\right)\theta \gg 1 \tag{C.3}$$

$$\frac{Pe_{\mathrm{Lm}}^2}{2\alpha_{\mathrm{L}}}\left(\frac{1}{Pe_{\mathrm{Rm}}} + \frac{1}{Pe_{\mathrm{Lm}} Pe_{\mathrm{Rm}}}\right) L^*\theta \gg 1 \tag{C.4}$$

Appendix D

The resistance offered by the packing to a flowing fluid according to the Darcy equation is given by

$$u = \bar{u} + \tilde{u} = -\frac{K_{\mathrm{r}}}{\mu}\frac{\partial P}{\partial z} = -\frac{(\bar{K}_{\mathrm{r}} + \tilde{K}_{\mathrm{r}})}{\mu}\frac{\partial P}{\partial z} \tag{D.1}$$

where $K_{\mathrm{r}} = K_{\mathrm{p}}/\varepsilon$; K_{p} is the permeability of the porous medium and $\partial P/\partial z$ is the pressure gradient in the flow direction.

Using Eq. (D.1), the velocity perturbation $\tilde{u}$ is related to the perturbation in the permeability $\tilde{K}_{\mathrm{r}}$ by

$$\frac{\tilde{u}}{\bar{u}} \cong \frac{\tilde{K}_{\mathrm{r}}}{\bar{K}_{\mathrm{r}}} \tag{D.2}$$

The same result was also obtained in ref. [75]. The longitudinal dispersion coefficient can be written in the elementary form (molecular diffusion effect was neglected for simplicity)

$$D_{\mathrm{L}} = \alpha_{\mathrm{L}} u \tag{D.3}$$

Using Eqs. (D.2) and (D.3), the perturbation in D_{L} can be approximated by

$$\tilde{D}_{\mathrm{L}}^* \cong \alpha_{\mathrm{L}}\bar{u}\frac{\tilde{K}_{\mathrm{r}}}{\bar{K}_{\mathrm{r}}} \tag{D.4}$$

The porosity variation shows an oscillatory variation from the wall [18] and Eq. (D.5) is an empirical fit of these data

$$\varepsilon(Y) = 0.38 + 0.62\exp(-1.70Y^{0.434})\cos(6.67Y^{1.13}) \tag{D.5}$$

where

$$Y = \frac{(1-\zeta)R}{2a} \tag{D.6}$$

The relation between the permeability variation and the void fraction is given by [76]

$$K_{\mathrm{r}} = \frac{K_{\mathrm{p}}}{\varepsilon} = \bar{K}_{\mathrm{r}} + \tilde{K}_{\mathrm{r}} = \frac{d_{\mathrm{p}}^2}{180}\frac{\varepsilon^2}{(1-\varepsilon)^2} \tag{D.7}$$

The perturbation $\tilde{K}_{\mathrm{r}}$ can be presented as

$$\frac{\tilde{K}_{\mathrm{r}}}{\bar{K}_{\mathrm{r}}} = \frac{\varepsilon^2}{2[(1-\varepsilon)^2\int_0^1 \zeta\varepsilon^2/(1-\varepsilon)^2\mathrm{d}\zeta]} - 1 \tag{D.8}$$

Eq. (16) can be re-writen as

$$\frac{\partial \bar{C}}{\partial \theta} = K_0(\theta)\frac{\partial^2 \bar{C}}{\partial x_1^2} + K_2(\theta)\frac{\partial^3 \bar{C}}{\partial x_1^3} + K_3(\theta)\frac{\partial^3 \bar{C}}{\partial x_1^2 \partial \theta} + K_4(\theta)\frac{\partial^4 \bar{C}}{\partial x_1^4} + K_5(\theta)\frac{\partial^4 \bar{C}}{\partial x_1^3 \partial \theta} \tag{D.9}$$

where $K_0(\theta)$–$K_5(\theta)$ are the same in (B.2)–(B.7) with $\tilde{\varepsilon} = 0$ and $\bar{\varepsilon} = 1$. The different moments of the distribution which corresponds to a pulse injection of tracer at $x = 0$ when $t = 0$ are found from [6]

$$\frac{\mathrm{d}M_p}{\mathrm{d}\theta} = K_0(\theta)p(p-1)M_{p-2} - K_2(\theta)p(p-1)(p-2)M_{p-3} + K_3(\theta)p(p-1)\frac{\mathrm{d}M_{p-2}}{\mathrm{d}\theta} + K_4(\theta)p(p-1)(p-2)(p-3)M_{p-4} \tag{D.10}$$

Normalizing the moments with M_0 (=constant) and integrating w.r.t. θ, the main features of the distribution are

Mean

$$\mu_1 = 0 \tag{D.11}$$

Variance

$$\mu_2 = 2\sum_{m=1}^{\infty} \frac{\overline{\tilde{u}J_0(\beta_m, \zeta)}}{\lambda N(\beta_m)} \left(\theta + \frac{\mathrm{e}^{-\lambda\theta}}{\lambda} - \frac{1}{\lambda}\right) \int_0^1 \zeta J_0(\beta_m, \zeta)\tilde{u}\,\mathrm{d}\zeta + \frac{2\theta}{Pe_{\mathrm{Lm}}} \tag{D.12}$$

Skewness

$$\Gamma = \frac{\mu_3}{\mu_2^{3/2}} \tag{D.13}$$

Kurtosis

$$\Delta = \frac{\mu_4}{\mu_2^2} \tag{D.14}$$

where

$$\mu_3 = -6\int_0^{\theta} K_2(\theta) \tag{D.15}$$

$$\frac{\mu_4}{\mu_2^2} - 3 = \frac{24}{\mu_2^2}\left(\int_0^{\theta} K_4(\theta) + \int_0^{\theta} K_0(\theta)K_3(\theta)\right) \tag{D.16}$$

The integrals in Eqs. (18), (19) and (D.12)–(D.16) are evaluated using the functions in Eqs. (D.2), (D.4) and (D.8) as

$$\frac{D_{\mathrm{L}}(\theta)}{D_{\mathrm{L}}(\infty)} = \frac{4Pe_{\mathrm{Rm}}\sum_{m=1}^{\infty}(\mathrm{Area}/(\beta_m J_0(\beta_m, \zeta)))^2(1 - \mathrm{e}^{-\lambda\theta}) + 1/Pe_{\mathrm{Lm}}}{4Pe_{\mathrm{Rm}}\sum_{m=1}^{\infty}(\mathrm{Area}/(\beta_m J_0(\beta_m, \zeta)))^2 + 1/Pe_{\mathrm{Lm}}} \tag{D.17}$$

$$\frac{V(\theta)}{V(\infty)} = \frac{4Pe_{\mathrm{Rm}}^2\sum_{m=1}^{\infty}(\mathrm{Area}/(\beta_m^2 J_0(\beta_m, \zeta)))^2(1 - (1+\lambda\theta)\,\mathrm{e}^{-\lambda\theta})}{4Pe_{\mathrm{Rm}}^2\sum_{m=1}^{\infty}(\mathrm{Area}\ 0/(\beta_m^2 J_0(\beta_m, \zeta)))^2} \tag{D.18}$$

$$\mu_2 = 2\left(4Pe_{\mathrm{Rm}}\sum_{m=1}^{\infty}\left(\frac{\mathrm{Area}}{\beta_m J_0(\beta_m, \zeta)}\right)^2\left(\theta - \frac{1}{\lambda} + \frac{\mathrm{e}^{-\lambda\theta}}{\lambda}\right) + \frac{\theta}{Pe_{\mathrm{Lm}}}\right) \tag{D.19}$$

$$\Gamma = \frac{48\left((\alpha Pe_{\mathrm{Rm}}/Pe_{\mathrm{Lm}})\sum_{m=1}^{\infty}(\mathrm{Area}/(\beta_m J_0(\beta_m, \zeta)))^2(\theta - (1/\lambda) + (\mathrm{e}^{-\lambda\theta}/\lambda))\right)}{(2)^{3/2}\left(4Pe_{\mathrm{Rm}}\sum_{m=1}^{\infty}(\mathrm{Area}/(\beta_m J_0(\beta_m, \zeta)))^2(\theta - (1/\lambda) + (\mathrm{e}^{-\lambda\theta}/\lambda)) + \theta/Pe_{\mathrm{Lm}}\right)^{3/2}} \tag{D.20}$$

$$\Delta = 3 + \frac{24}{\mu_2^2}\left\{4\frac{Pe_{\mathrm{Rm}}^2}{Pe_{\mathrm{Lm}}}\sum_{m=1}^{\infty}\left(\frac{\text{Area}}{\beta_m^2 J_0(\beta_m,\zeta)}\right)^2\left(\theta - \frac{2}{\lambda} + \frac{2e^{-\lambda\theta}}{\lambda} + \theta\,\mathrm{e}^{-\lambda\theta}\right) + 4\frac{Pe_{\mathrm{Rm}}}{Pe_{\mathrm{Lm}}^2}\sum_{m=1}^{\infty}\left(\frac{\text{Area}}{\beta_m J_0(\beta_m,\zeta)}\right)^2 \times \left(\theta - \frac{1}{\lambda} + \frac{\mathrm{e}^{-\lambda\theta}}{\lambda}\right) - \int_0^{\theta} K_1(\theta)K_3(\theta)\,\mathrm{d}\theta\right\} \tag{D.21}$$

$$\text{Area} = \int_0^1 \zeta J_0(\beta_m,\zeta)\tilde{u}\,\mathrm{d}\zeta \tag{D.22}$$

Appendix E

The three term Edgeworth series expansion has been used to approximate the concentration distribution

$$\frac{\sqrt{2\pi\mu_2}}{\mu_0}\bar{C} = \exp\left(-\frac{\tau^2}{2}\right)\left[1 + \frac{\lambda_3}{6}H_3(\tau) + \frac{\lambda_4}{24}H_4(\tau) + \frac{\lambda_3^2}{72}H_6(\tau)\right]; \tag{E.1}$$

$$\tau = \frac{x_1}{\sigma} \tag{E.2}$$

$$\lambda_2 = \mu_2; \qquad \lambda_3 = \Gamma; \quad \lambda_4 = \Delta - 3 \tag{E.3}$$

$$H_3(\tau) = \tau^3 - 3\tau \qquad H_4(\tau) = \tau^4 - 6\tau^2 + 3 \qquad H_6(\tau) = \tau^6 - 15\tau^4 + 45\tau^2 - 15 \tag{E.4}$$

References

[1] J.R.F. Carvalho, J.M.P.Q. Delgado, Overall map and correlation of dispersion data for flow through granular packed beds, Chem. Eng. Sci. 60 (2005) 365–375.
[2] J.M.P.Q. Delgado, A critical review of dispersion in packed beds, Heat Mass Trans. 42 (2006) 279–310.
[3] B.C. Chandrasekhara, N. Rudraiah, S.T. Nagaraj, Velocity and dispersion in porous-media, Int. J. Eng. Sci. 18 (1980) 921–929.
[4] N. Han, J. Bhakta, R.G. Carbonell, Longitudinal and lateral dispersion in packed beds, effect of column length and particle size distribution, AIChE J. 31 (1985) 277–387.
[5] G.I. Taylor, Dispersion of solute matter in solvent flowing slowly through a tube, Proc. R. Soc. Lond. A 219 (1953) 186–203.
[6] R. Aris, On the dispersion of a solute in a fluid flowing through a tube, Proc. R. Soc. Lond. A 235 (1956) 67–77.
[7] A.E. Scheidegger, An evaluation of the accuracy of the diffusivity equation for describing miscible displacement in porous media, in: Proceedings of Theory of Fluid Flow in Porous Media Conference, University of Oklahoma, 1959, pp. 101–116.
[8] S.E. Silliman, E.S. Simpson, Laboratory evidence of the scale effect in dispersion of solutes in porous-media, Water Resour. Res. 23 (1987) 1667–1673.
[9] S. Oswald, W.A.G. Kinzelbach, G. BRIX, Observation of flow and transport process in artificial porous media via magnetic resonance imaging in three dimensions, Geoderma 80 (1997) 417–429.
[10] L.W. Gelhar, A.L. Gutjahr, R.L. Naff, Stochastic analysis of macrodispersion in a stratified aquifer, Water Resour. Res. 15 (1979) 1387–1397.
[11] S.P. Neuman, C.L. Winter, C.M. Newman, Stochastic theory of field-scale Fickian dispersion in anistropic porous media, Water Resour. Res. 23 (1987) 453–466.
[12] R. Schumer, D.A. Benson, M.M. Meerschaert, B. Baeumer, Fractal mobile/immobile solute transport, Water Resour. Res. 39 (2003) 1296, doi:10.1029/2003WR002141.
[13] L. Pang, B. Hunt, Solution and verification of a scale-dependent dispersion model, J. Contam. Hydrol. 53 (2001) 21–39.
[14] J.F. Piekens, G.E. Grisak, Modelling of scale-dependent dispersion in hydro geologic systems, Water Resour. Res. 17 (1981) 1701–1711.
[15] M. Levy, B. Berkowitz, Measurement and analysis of non-Fickian dispersion in heterogeneous porous media, J. Contam. Hydrol. 64 (2003) 203–226.
[16] A. Cortis, C. Gallo, H. Scher, B. Berkowitz, Numerical simulation of non-Fickian transport geological formations with multiple-scale heterogeneities, Water Resour. Res. 40 (2004) (Art. No. W04209 April 21, 2004).
[17] C.W. Fetter, Contaminant Hydrology, Macmillan, New York, 1993, pp. 71–109.
[18] R.F. Benenati, C.B. Brosilow, Void fraction distribution in beds of spheres, AIChE J. 8 (1962) 359–362.
[19] R.S. Maier, D.M. Kroll, R.S. Bernard, S.E. Howington, J.F. Peters, H.T. Davis, Hydrodynamic dispersion in confined packed beds, Phys. Fluids 15 (2003) 3795–3815.
[20] D.L. Koch, J.F. Brady, Anomalous diffusion in heterogeneous porous-media, Phys. Fluids 31 (1988) 965–973.
[21] J.D. Seymour, J.P. Gage, S.L. Codd, R. Gerlach, Anomalous fluid transport in porous induced by biofilm growth, Phys. Rev. Lett. 93 (2004) 1–4.
[22] D.A. Verganelakis, J. Crawshaw, M.L. Jhons, M.D. Mantle, U. Scheven, A.J. Sederman, L.F. Gladden, Displacement propagators of brine flowing within different types of Sedimentary rock, Magn. Reson. Imaging 23 (2005) 349–351.
[23] J.D. Seymour, P.T. Callaghan, Generalized approach to NMR analysis of flow and dispersion in porous media, AIChE J. 43 (1997) 2096–2111.
[24] S. Stapf, K.J. Packer, R.G. Graham, J.-F. Thovert, P.M. Alder, Spatial correlations and dispersion for fluid transport through packed glass beads studied by pulsed field-gradient NMR, Phys. Rev. E 58 (1998) 6206–6221.
[25] J.J. Tessier, K.J. Packer, J.-F. Thovert, P.M. Adler, NMR measurements and numerical simulation of fluid transport in porous solids, AIChE J. 43 (1997) 1653–1661.
[26] A. Cenedese, P. Viotti, Lagrangian analysis of non-reactive pollutant dispersion in porous media by means of the particle image velocimetry technique, Water Resour. Res. 32 (1996) 2329–2343.
[27] P. Viotti, Scaling properties of tracer trajectories in a saturated porous medium, Trans. Porous Media 27 (1997) 1–16.
[28] J. Salles, J.-F. Thovert, R. Delannay, L. Prevors, J.-L. Auriault, P.M. Alder, Taylor dispersion in porous media-determination of the dispersion tensor, Phys. Fluids A Fluid Dynam. 10 (1993) 2348–2376.

[29] C.P. Lowe, D. Frenkel, Do hydrodynamic dispersion coefficients exist? Phys. Rev. Lett. 77 (1996) 4552–4555.
[30] R.S. Maier, D.M. Kroll, R.S. Bernard, S.E. Howington, J.F. Peters, H.T. Davis, Enhanced dispersion in cylindrical packed beds, Philos. Trans. R. Soc. Lond. A 360 (2002) 497–506.
[31] K.B. Bischoff, O. Levenspile, Fluid dispersion—generalization and comparison of mathematical models: II, Chem. Eng. Sci. 17 (1962) 257–264.
[32] D.L. Koch, J.F. Brady, Nonlocal dispersion in porous media—non mechanical effects, Chem. Eng. Sci. 42 (1987) 1377–1392.
[33] R.S. Maier, D.M. Kroll, R.S. Bernard, S.E. Howington, J.F. Peters, H.T. Davis, Pore scale simulation of dispersion, Phys. Fluids 12 (2000) 2065–2079.
[34] R.G. Carbonell, Flow nonuniformities in packed beds—effect on dispersion, Chem. Eng. Sci. 35 (1980) 1347–1456.
[35] M.N. Ozisik, Heat Conduction, John Wiley and Sons, New York, 1980, p. 522.
[36] B.H. Chen, A.F. McMillan, S.T. Wang, An analytical solution for dispersion in packed-beds with low bed-to-particle diameter ratios, Chem. Eng. Sci. 38 (1983) 257–263.
[37] W.R. Young, S. Jones, Shear dispersion, Phys. Fluids A 3 (1991) 1087–1101.
[38] S. Haber, R. Mauri, Lagrangian approach to time-dependent laminar dispersion in rectangular conduits, Part 1. Two-dimensional flows, J. Fluid Mech. 190 (1988) 201–215.
[39] M. Dentz, J. Carrera, Mixing and spreading in stratified flow, Phys. Fluids 19 (2007) 017107.
[40] C.W.J. Berentsen, M.L. Verlaan, C.P.J.W. Van Kruijdijk, Upscaling and reversibility of Taylor dispersion in heterogeneous porous media, Phys. Rev. E 71 (2005) 046308.
[41] G.I. Taylor, Conditions under which dispersion of a solute in a stream of solvent can be used to measure molecular diffusion, Proc. R. Soc. Lond. A 225 (1954) 473–477.
[42] P.V. Danckwerts, Continuous flow systems, Chem. Eng. Sci. 2 (1953) 1–13.
[43] H. Kramers, G. Alberda, Frequency response analysis of continuous flow systems, Chem. Eng. Sci. 2 (1953) 173–181.
[44] G.L. Jacques, T. Vermeulen, Longitudinal dispersion in solvent- extraction columns: Peclet numbers for random and ordered packings. Univ. California Rad Lab. Rep. No. 8029, US Atomic Energy Commission, 1958, Washington, DC.
[45] J.J. Carberry, R.H. Bretton, Axial dispersion of mass in flow through fixed beds, AIChE J. 4 (1958) 367–375.
[46] E.A. Ebach, R.R. White, Mixing of fluids flowing through beds of packed solids, AIChE J. 4 (1958) 161–169.
[47] D.A. Strang, C.J. Geankopolis, Longitudinal diffusivity of liquids in packed beds, Ind. Eng. Chem. 50 (1958) 1305.
[48] E.J. Cairns, J.M. Prausnitz, Longitudinal mixing in packed beds, Chem. Eng. Sci. 12 (1960) 20–34.
[49] A.W. Liles, C.J. Geankopolis, Axial diffusion of liquids in packed beds and End effects, AIChE J. 6 (1960) 591.
[50] D. Harrison, M. Lane, D.J. Walne, Axial dispersion of liquid on a column of spheres, Trans. IChemE 40 (1962) 214–220.
[51] J.W. Hiby, Longitudinal dispersion in single-phase liquid flow through ordered and random packings, interact between Fluid & Particles, Lond. Inst. Chem. Eng. (1962) 312–325.
[52] A. Hennico, G. Jacques, T. Vermeulen, Longitudinal dispersion in single-phase liquid flow through ordered and random packings, Lawrence Rad Lab. Rept. UCRL, 1963, 10696.
[53] H.-O. Pfannkuch, Contribution a l'e'tude des de'placements de fluids miscibles dans un milieu poreux, Revue de l'institut du petro 18 (1963) 215–270.
[54] S.S. Miller, C.J. King, Axial dispersion in liquid flow through backed beds, AICHE J. 12 (1966) 767–773.
[55] W.D. Smith, R.H. Bretton, Paper presented at AIChE Houston Meeting, Texas, 1967.
[56] S.F. Chung, C.Y. Wen, Longitudinal dispersion of liquid flowing through fixed and fluidized beds, AIChE J. 14 (1968) 857–866.
[57] T. Miyauchi, T. Kikuchi, Axial dispersion in packed beds, Chem. Eng. Sci. 30 (1975) 343–348.
[58] J.R.F. Carvalho, J.M.P.Q. Delgado, The effect of fluid properties on dispersion in flow through packed beds, AIChE J. 49 (2003) 1980–1985.
[59] J.R. McHenry, R.H. Wilhelm, Axial mixing of binary gas mixtures flowing in a random bed of spheres, AIChE J. 3 (1957) 83–91.
[60] R.J. Blackwell, J.R. Rayne, W.M. Terry, Factors influencing the efficiency of miscible displacement, AIME Petroleum Trans. 216 (1959) 1–8.
[61] F. DeMaria, R.R. White, Transient response study of a gas flowing through irrigated packing, AIChE J. 6 (1960) 473–481.
[62] R.J. Sinclair, O.E. Potter, The dispersion of gas in flow through a bed of packed solids, Trans. IChemE 43 (1965) T3–T9.
[63] E.V. Evans, C.N. Kenney, Gaseous dispersion in packed beds at low Reynolds numbers, Trans. Inst. Chem. Eng. 44 (1966) T189–T197.
[64] M.F. Edward, J.F. Richardson, Gas dispersion in packed beds, Chem. Eng. Sci. 23 (1968) 109–123.
[65] L.Z. Balla, T.W. Weber, Axial dispersion of gases in packed beds, AIChE J. 15 (1969) 146–149.
[66] J.C. Urban, A. Gomezplata, Axial dispersion coefficients in packed beds at low Reynolds numbers, Can. J. Chem. Eng. 47 (1969) 353–363.
[67] D.S. Scott, W. Lee, J. Papa, The measurement of transport coefficients in gas–solid heterogeneous reactions, Chem. Eng. Sci. 29 (1974) 2155–2167.
[68] T.C.S. Hsiang, H.W. Haynes, Axial dispersion in small diameter beds of large spherical-particles, Chem. Eng. Sci. 32 (1977) 678–681.
[69] A.H. Benneker, A.W. Kronberg, J.W. Post, A.G.J. Van Der Han, K.R. Westerterp, Axial dispersion in gases flowing through a packed bed at elevated pressures, Chem. Eng. Sci. 15 (1996) 2099–2108.
[70] D. Yu, K. Jackson, T.C. Harmon, Dispersion and diffusion in porous media under supercritical conditions, Chem. Eng. Sci. 54 (1999) 357–367.
[71] D. Yu, Solute pulse dispersion in soil columns: a comparison of supercritical CO_2, gaseous and aqueous systems, Ph.D. Thesis, University of California, 1998.
[72] C.S. Tan, D.C. Liou, Axial dispersion of supercritical carbon dioxide in packed beds, Ind. Eng. Chem. Res. 28 (1989) 1246–1250.
[73] T. Daszkowski, G. Eigenberger, A re-evaluation of fluid-flow, heat-transfer and chemical-reaction in catalyst filled tubes, Chem. Eng. Sci. 47 (1992) 2245–2250.
[74] J.N. Papageorgiou, G.F. Froment, Simulation models accounting for radial voidage profiles in fixed bed reactors, Chem. Eng. Sci. 50 (1995) 3043–3056.
[75] D.A. Neuman, A.V. Kuzentsov, Effects of heterogenity in forced convection in a porous medium: parallel plate channel or circular duct, Int. J. Heat Mass Trans. 43 (2000) 4119–4134.
[76] P.C. Carman, Fluid flow through a granular bed, Trans. Inst. Chem. Eng. 15 (1937) 150–167.
[77] P.C. Chatwin, Approach to normality of concentration distribution of a solute in a solvent flowing along a straight pipe, J. Fluid Mech. 43 (1970) 321.
[78] D.R.F. Harleman, R.R. Rumer, Longitudinal and lateral dispersion in an isotropic porous medium, J. Fluid Mech. 16 (1963) 385–394.
[79] M. Kendall, Kendall's Advanced Theory of Statistics, fifth ed., Charles Griffin Company Limited, 1987, pp. 222–226.